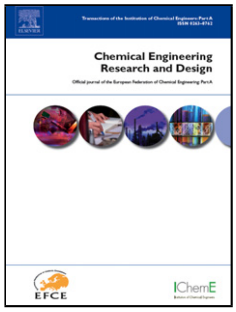

Title: INfluence of drag and turbulence modelling on CFD predictions of solid liquid suspensions in stirred vessels

Author: A. Tamburini A. Cipollina G. Micale A. Brucato M. Ciofalo

PII: S0263-8762(13)00440-1
DOI: http://dx.doi.org/doi:10.1016/j.cherd.2013.10.020
Reference: CHERD 1399

To appear in:

Received date: 30-7-2013
Revised date: 3-10-2013
Accepted date: 16-10-2013

Please cite this article as: Tamburini, A., Cipollina, A., Micale, G., Brucato, A., Ciofalo, M.,INfluence of drag and turbulence modelling on CFD predictions of solid liquid suspensions in stirred vessels, *Chemical Engineering Research and Design* (2013), http://dx.doi.org/10.1016/j.cherd.2013.10.020

HIGHLIGHTS

- Solid-liquid suspensions in stirred tanks are investigated by CFD.
- Partial to complete suspension conditions were studied.
- Alternative models for inter-phase drag force and turbulence closure are tested.
- Results are validated against a large number of experimental data.
- Asymmetric k-ε model plus Brucato et al correction is found to be a good compromise.

INFLUENCE OF DRAG AND TURBULENCE MODELLING ON CFD PREDICTIONS OF SOLID LIQUID SUSPENSIONS IN STIRRED VESSELS

A. Tamburini [a], A. Cipollina [a], G. Micale [a]*, A. Brucato[a], M. Ciofalo[b]

[a] *Dipartimento di Ingegneria Chimica, Gestionale, Informatica, Meccanica*

[b] *Dipartimento Energia, Ingegneria dell'Informazione e Modelli Matematici*

Università di Palermo, Viale delle Scienze Ed. 6, 90128 Palermo (ITALY)

* Corresponding author: giorgiod.maria.micale@unipa.it

Abstract. Suspensions of solid particles into liquids within industrial stirred tanks are frequently carried out at an impeller speed lower than the minimum required for complete suspension conditions. This choice allows power savings which usually overcome the drawback of a smaller particle-liquid interfacial area. Despite this attractive economical perspective, only limited attention has been paid so far to the modelling of the partial suspension regime.

In the present work two different baffled tanks stirred by Rushton turbines were simulated by employing the Eulerian-Eulerian Multi Fluid Model (MFM) along with either the Sliding Grid algorithm (transient simulations) or the Multiple Reference Frame technique (steady state simulations). In particular, a comparison of alternative modelling approaches for inter-phase drag force and turbulence closure is presented. The results are evaluated against a number of experimental data concerning sediment features (amount and shape) and local axial profiles of solids concentration, with emphasis on the partial suspension regime.

Results show that some of the approaches commonly adopted to account for dense particle effects or turbulent fluctuations of the volumetric fractions may actually lead to substantial discrepancies from the experimental data. Conversely simpler models which do not include such additional effects give the best overall predictions in the whole range of partial to complete suspension conditions.

Key words: Computational Fluid Dynamics (CFD); stirred tank; solid liquid suspension; drag force; turbulence model; multiphase flow.

1. INTRODUCTION AND LITERATURE REVIEW

1.1 Partial and complete suspension conditions

Many research efforts have been devoted to the investigation of solid-liquid stirred tanks in the last decades (Zwietering, 1958; Nienow, 1968; Bourne and Sharma, 1974; Yamazaki et al, 1986; Barresi and Baldi, 1987; Oldshue and Sharma, 1992; Armenante et al., 1998; Micale et al., 2000; Rieger, 2000; Angst and Kraume, 2006; Sardeshpande et al., 2009; Tamburini et al., 2009b,2013a; Jirout and Rieger, 2011; Montante et al., 2012). The minimum impeller speed for complete suspension conditions, N_{js} is the most investigated topic since it is known to represent a good compromise between the reduction of agitation costs and the enhancement of mass transfer processes. Many studies focus on the proposal of methods to measure N_{js} (Zwietering, 1958, Musil and Vlk, 1978; Bohnet and Niesmak, 1980; Rewatkar et al., 1991; Micale et al., 2002; Zhu and Wu, 2002; Jirout et al., 2005; Ren et al., 2008; Brucato et al., 2010; Tamburini et al., 2011c,2012c; Selima et al., 2008) or CFD models for its prediction (Kee and Tan, 2002; Wang et al., 2004; Murthy et al., 2007; Hosseini et al., 2010; Tamburini et al., 2012a).

Despite this traditional interest for the assessment of N_{js}, in many industrial solid-liquid stirred reactors the best compromise between cost reduction and process efficiency is achieved by operating at an impeller speed lower than N_{js} (Oldshue, 1983; Rieger et al., 1988; Van der Westhuizen and Deglon, 2007; Jafari et al., 2012; Wang et al., 2012). Van der Westhuizen and Deglon (2007) investigated a mechanical flotation cell and stated that particles sedimentation and associated losses may become drastic only when the system is operated at an $N < 0.6\ N_{js}$ (under gassed condition). Jafari et al. (2012) reported data concerning the operation of an industrial slurry reactor for the gold cyanidation process at $N = 0.8\ N_{js}$; a choice which (i) did not appreciably affect the reaction selectivity and process yield and (ii) allowed a substantial reduction of energy consumption with respect to complete suspension conditions. Also, they reported that a decrease of

~0.55 M$/year in product value due to operating at $N = 0.5\ N_{js}$ corresponded to an energy saving of ~1M$/year, with a ~0.45 M$/year increase in net profit.

In this regard, the availability of data on the partial suspension conditions may be very useful for the industry. Such information could allow economical analyses to be performed leading to the optimal choice of N. Notwithstanding the interest expressed so far at the industrial level for partial suspension conditions, only a few data can be found in the literature for this particular regime and many of them were collected with different aims. For instance, except for a few cases (Tamburini et al., 2011a,b, 2012b), all literature works presenting CFD data on systems under partial suspension conditions are devoted to the evaluation of N_{js} (Kee and Tan, 2002; Oshinowo and Bakker, 2002; Wang et al., 2004; Ochieng and Lewis, 2006; Murthy et al., 2007; Kasat et al., 2008; Panneerselvam et al., 2008; Hosseini et al., 2010): most of the criteria adopted in the literature to estimate N_{js} require data at $N < N_{js}$ and $N > N_{js}$ thus leading to the necessity of performing simulations under partial suspension conditions. However, none of these works fully investigated the partial suspension regime.

A universal CFD model capable to manage all the types of solid-liquid suspensions within stirred tanks does not exist yet. For the case of complete suspension, it is possible to find in the literature different formulations for the inter-phase drag force treatment as well as for the turbulence closure.

1.2 Inter-phase drag force

The inter-phase drag force is one of the most crucial factors affecting both solids suspension and distribution. Gidaspow's *dense particle effect* (Gidaspow, 1994) is the most accepted formulation of the inter-phase drag force which takes into account the particle-particle interaction effect (Gidaspow, 1994; Ochieng and Onyango, 2008; Scully and Frawley, 2011): according to this formulation, the higher the local solid volume fraction, the higher the inter-phase drag force as a consequence of more intense particle-particle interactions. When the solid loading is very high, the

adoption of Ergun's equation (Ergun, 1952) for the inter-phase drag force is commonly suggested (CFX-4 Documentation, 1994; Ochieng and Onyango, 2008) although it was originally formulated for the case of fixed beds of particles. In some cases, the two previous approaches are simultaneously employed for the simulation of the same system, the former being employed in the domain regions with low solid volume fractions and the latter in the domain regions with higher solid volume fractions (Gidaspow, 1994; CFX-4 Documentation, 1994; Ochieng and Onyango, 2008) thus leading to a discontinuity in the relation between inter-phase drag force and solid volume fraction. Recently, Tamburini et al. (2009a) proposed a piecewise correlation employing the two above formulations along with a linear interpolation between them for an intermediate range of solid volume fractions thereby avoiding any discontinuity and providing a monotonic behaviour in the inter-phase drag force vs solid volume fraction relation.

1.3 Turbulence closure

As far as the turbulence closure is concerned, the k-ε turbulence model (along with the Eulerian-Eulerian treatment of the two phase system) is the most widely employed for solid-liquid systems. In particular, four main two-phase extensions of the standard k-ε turbulence model (*homogeneous*, *per phase*, *dispersed* and *asymmetric*) can be encountered in the literature.

- In the *homogeneous* approach, only one k and one ε equations are solved, where the physical properties of the mixture are adopted: the two phases share the same k and ε value and the transport equations for k and ε have no inter-phase turbulence transfer terms.
- In the *per phase*, or *phase-specific*, formulation, the turbulence model equations are solved for each phase. Additional terms referring to the modelling of inter-phase transport of k and ε have to be included in the equations relevant to each phase.
- Alternatively, in the *dispersed* approach, suitable for dilute suspensions, fluctuating quantities of the dispersed phase are computed as functions of the mean characteristics of

the continuous phase and the ratio of the particle relaxation time and eddy-particle interaction time (Gosman et al., 1992). Continuous phase turbulence is modelled using the standard k-ε model including extra terms which account for the influence of the dispersed phase on the continuous one (Feng et al., 2012). Predictions of turbulence quantities for the dispersed phases are obtained using the Tchen theory of dispersion of discrete particles by homogeneous turbulence (Hinze, 1975).

- Recently Tamburini et al. (2011a) proposed the adoption of the *asymmetric* k-ε turbulence model and applied it to dense solid-liquid suspensions at $N \leq N_{js}$: according to this approach, since many particles may be unsuspended under partial suspension conditions, only the turbulence of the liquid phase was accounted for and no turbulent viscosity was calculated for the solid phase.

Montante and Magelli (2005) compared the first three formulations. They observed that using more computationally demanding approaches like the *per phase* formulation does not lead to any significant improvement over the homogeneous formulation. Furthermore, the *homogeneous* k-ε turbulence model provides a satisfactory representation of the solids distribution throughout the vessel for a number of cases involving dense suspensions in stirred tanks provided that $N \geq N_{js}$ (Montante et al., 2001; Micale et al., 2004; Montante and Magelli, 2005; Khopkar et al., 2006; Kasat et al., 2008; Tamburini et al., 2009a).

On the basis of the above considerations, the present work aims at comparing different CFD models including alternative formulations of either the inter-phase drag force or the turbulence closure in order to identify the best modelling procedure to deal with the incomplete suspension regime.

2 EXPERIMENTAL DATA

The data employed for the validation of the CFD simulations derive from experiments made by the authors (Tamburini et al., 2011a) and from the literature (Micheletti et al., 2003). Such data are relevant to two very similar systems both consisting of solid-liquid suspensions in a cylindrical flat-bottomed baffled tank stirred by a standard six-bladed Rushton turbine.

A) The first tank, sketched in Fig. 1, has internal diameter T equal to 0.19 m, impeller diameter D equal to T/2 and impeller clearance C equal to T/3, and is filled up to a height H=T.

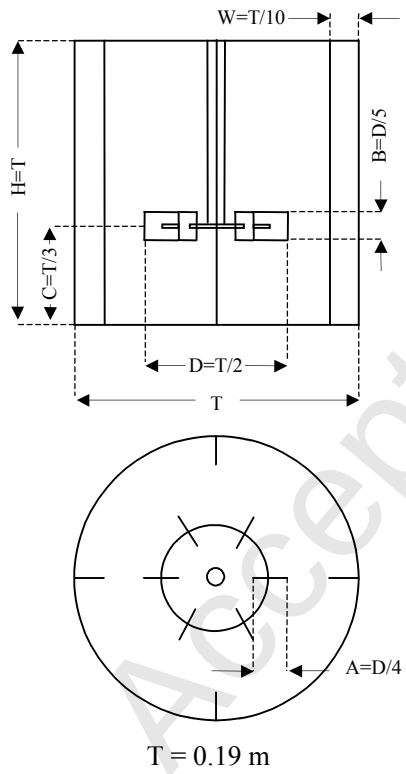

Fig. 1: System A

The experimental data (Tamburini et al., 2011a) regarding this system are relevant to three different suspensions of glass ballottini (ρ_β=2500 kg/m^3) in deionized water with diameter range and mass fractions of:

- 212-250 μm, 33.8% w_{solid}/w_{liquid} (referred as w/w in the following);

- 212-250 μm, 16.9% w/w;

- 500-600 μm, 33.8% w/w.

These data provide the suspension curve (i.e. the mass fraction of suspended particles x_{susp} against the impeller speed N) and the height of the sediment h_{sed} visible on the lateral wall midway between two subsequent baffles.

B) The second tank, investigated by Micheletti et al. (2003), is a flat bottomed tank with T=H=0.29m, impeller diameter D equal to T/3 and impeller clearance C equal to T/3.

The experimental data regard a suspension in deionized water of 600-710 μm glass particles (ρ_β=2470 kg/m^3) with 25% w/w.

These data provide axial profiles of solid concentration. More precisely, local steady state solid concentrations measurements were performed by a conductivity probe at a radial position R/T=0.35, midway between subsequent baffles and at different heights of the tank.

The above experimental data are the only ones available in the literature concerning particle distribution under partial suspension conditions. This is the main reason why all the presently reported simulations were limited to a Rushton turbine.

The void fraction of the particle bed lying on the bottom under no agitation conditions was estimated to be about 40% for both systems on the basis of the literature (Tamburini et al., 2011a) and specific measurements.

3 MODELLING

RANS simulations of the systems described in the previous section were performed by adopting the Eulerian-Eulerian Multi Fluid Model (MFM), available as a standard option in the commercial finite volume CFD code Ansys$^{(R)}$ CFX4.4. With respect to more recent releases, this code version

offers a greater flexibility in designing user-defined routines for non standard problems, thus, it has been extensively applied by the present authors to a variety of non standard CFD problems (Micale et al., 1999; Di Piazza and Ciofalo, 2002). In the present work, the choice of this code allowed the implementation of the Excess Solid Volume Correction solids redistribution algorithm described in section 4.

According to the MFM fundamentals, the two phases are treated as two interpenetrating continua: the continuity and momentum equations are solved for each phase, thus obtaining separate flow field solutions for the liquid and the solid phase simultaneously. The two phases share the same pressure field.

Different modelling approaches were implemented and tested in the present work: all the combinations simulated are summarized in Tab.1, while the main features of each combination (i.e. tested modelling approach) are classified and described in the following paragraphs.

	Additional terms arising from turbulence closure in continuity equation			**Interphase Drag Force in momentum equations**			**Turbulence Model**	
Modelling approach	No terms	Liquid phase only	Both phases	Standard (eq.6)	Gidaspow's dense particle effect	Gidaspow-Ergun Piecewise correlation	Homogeneous k-ε	Asymmetric k-ε
Reference Model	X			X				X
DPE	X				X			X
PwC	X					X		X
Homogeneous_no terms	X			X			X	
Homogeneous_2 terms			X	X			X	
Asymmetric_1 term		X		X				X

Table 1: Summary of the modelling approaches features

3.1 Reference Model

A very simple model was employed to evaluate its capability of predicting the whole set of the experimental data. As it will be better described in the following, this model accounts only for the turbulence of the liquid phase and adopts only a very standard formulation of the drag force. Moreover, also the turbulence fluctuations of the volumetric fractions are not taken into account. As a second step, more refined modelling approaches will be also tested. This simple model represents

the reference modelling approach with respect to which, all the other approaches can be regarded as modifications. It was already employed by the present authors (Tamburini et al., 2011a) and will be only briefly described in the following.

Continuity equations:

Assuming both phases to be incompressible, for each phase, the continuity equation is written as a function of the relevant volume fraction:

$$\rho_\alpha \frac{\partial}{\partial t}\left(r_\alpha\right)+\rho_\alpha \vec{\nabla}\cdot\left(r_\alpha \vec{U}_\alpha\right)=0 \tag{1}$$

$$\rho_\beta \frac{\partial}{\partial t}\left(r_\beta\right)+\rho_\beta \vec{\nabla}\cdot\left(r_\beta \vec{U}_\beta\right)=0 \tag{2}$$

where the subscripts α and β refer to the continuous and dispersed phases respectively, r is volumetric fraction, ρ is density and U is mean velocity.

Clearly,

$$r_\alpha + r_\beta = 1 \tag{3}$$

Momentum equations:

Assuming both phases to behave as Newtonian fluids, one has

$$\rho_\alpha \frac{\partial\left(r_\alpha \vec{U}_\alpha\right)}{\partial t}+\rho_\alpha \vec{\nabla}\cdot\left(r_\alpha \vec{U}_\alpha \otimes \vec{U}_\alpha\right)=\vec{\nabla}\cdot\left(r_\alpha\left(\mu_\alpha+\mu_{t\alpha}\right)\left(\vec{\nabla}\vec{U}_\alpha+\left(\nabla \vec{U}_\alpha\right)^T\right)\right)-r_\alpha \vec{\nabla}P+r_\alpha \rho_\alpha \vec{g}+\vec{M}_{\alpha\beta} \tag{4}$$

$$\rho_\beta \frac{\partial\left(r_\beta \vec{U}_\alpha\right)}{\partial t}+\rho_\beta \vec{\nabla}\cdot\left(r_\beta \vec{U}_\beta \otimes \vec{U}_\beta\right)=\vec{\nabla}\cdot\left(r_\beta \mu_\alpha\left(\vec{\nabla}\vec{U}_\beta+\left(\vec{\nabla}\vec{U}_\beta\right)^T\right)\right)-r_\beta \vec{\nabla}P+r_\beta \rho_\beta \vec{g}-\vec{M}_{\alpha\beta} \tag{5}$$

where g is gravity acceleration, μ is viscosity, μ_t is turbulent viscosity, P is pressure and M is the inter-phase momentum transfer term. Notably, M was considered to be equal to the drag force, while contributions due to other forces were neglected as suggested by the literature for similar

systems (Ljungqvist and Rasmuson, 2001; Fan et al., 2005; Fletcher and Brown, 2009; Sardeshpande et al., 2011). In particular, according to Fletcher and Brown (2009) the virtual mass and the lift forces have a negligible effect on the system dynamics; similarly, the Basset force in most cases is found to be much smaller than the drag force (Khopkar et al., 2006; Kasat et al., 2008). Also, Tatterson (1991) estimated virtual mass and lift forces to be much smaller than the drag force and, thus, to be negligible when $\rho_\beta/\rho_\alpha > 2$ (as in the present work).

Interphase Drag Force:

$$\vec{M}_{\alpha\beta} = C_{\alpha\beta}\left(\vec{U}_\beta - \vec{U}_\alpha\right) = \left[\frac{3}{4}\frac{C_{D,turb}}{d_p} r_\beta \rho_\alpha \left|\vec{U}_\beta - \vec{U}_\alpha\right|\right]\left(\vec{U}_\beta - \vec{U}_\alpha\right) \tag{6}$$

The particle drag coefficient based on two phases slip velocity was estimated by means of the Clift et al. correlation (1978):

$$C_{D,slip} = \frac{24}{\mathrm{Re}_p}\left(1 + 0.2\,\mathrm{Re}_p^{0.63}\right) \qquad \text{(for } \mathrm{Re_p} \le 1000\text{)} \tag{7a}$$

$$C_{D,slip} = 0.4 \qquad \text{(for } \mathrm{Re_p} > 1000\text{)} \tag{7b}$$

where Re_p is the slip velocity Reynolds number:

$$\mathrm{Re}_p = \frac{\rho_\alpha d_p \left|\vec{U}_\beta - \vec{U}_\alpha\right|}{\mu_\alpha} \tag{8}$$

The influence of the free stream turbulence on particle drag was accounted for by employing the correlation by Brucato et al. (1998),

$$C_{D,turb}^{Brucato} = C_{D,slip}\left[1 + 8.76\times10^{-4}\left(\frac{d_p}{\lambda}\right)^3\right] \tag{9}$$

where λ is the Kolmogorov length scale, calculated by

$$\lambda = \left(\nu^3/\varepsilon\right)^{0.25} \tag{10}$$

where the dissipation of turbulent kinetic energy ε is provided by the turbulence model.

Table 2 shows the correction of $C_{D,slip}$ provided by eq. 9, for the case of the *Reference model*. The values provided in the table are relevant to the average value of ε in the computational domain. Clearly, the correction is crucial for large particles and high impeller speeds.

SYSTEM A						**SYSTEM B**		
231 μm			550 μm			655 μm		
	Brucato et al. Correlation			Brucato et al. correlation			Brucato et al. correlation	
N [RPM]	**d_p/λ**	**$C_{D,turb}/C_{D,slip}$**	**N [RPM]**	**d_p/λ**	**$C_{D,turb}/C_{D,slip}$**	**N [RPM]**	**d_p/λ**	**$C_{D,turb}/C_{D,slip}$**
121	2.78	1.02	122	6.89	1.28	400	14.54	3.66
157	3.33	1.03	161	8.24	1.49	500	17.58	5.71
209	4.18	1.06	213	9.91	1.84	600	20.55	8.53
258	5.03	1.11	263	11.79	2.42	700	23.10	11.69
299	5.64	1.16	316	13.83	3.29	800	25.45	15.30
362	6.44	1.23	368	15.71	4.36	900	27.87	19.77
493	8.21	1.48	413	17.08	5.32	1000	29.68	23.68
			460	18.62	6.60	1100	32.57	30.95
			510	20.21	8.15			
			624	23.64	12.46			
			678	25.20	14.87			

Tab. 2: Influence of liquid free stream turbulence on drag coefficient.

<u>*k-ε* transport equations:</u>

$$\rho_\alpha \frac{\partial}{\partial t}\left(r_\alpha k_\alpha\right)+\vec{\nabla}\left[r_\alpha \rho_\alpha \vec{U}_\alpha k_\alpha - r_\alpha\left(\mu_\alpha+\frac{\mu_{t\alpha}}{\sigma_k}\right)\vec{\nabla}k_\alpha\right]=r_\alpha\left[\mu_{t\alpha}\vec{\nabla}\vec{U}_\alpha\left(\vec{\nabla}\vec{U}_\alpha+\left(\vec{\nabla}\vec{U}_\alpha\right)^T\right)-\rho_\alpha\varepsilon_\alpha\right] \quad (11)$$

$$\rho_\alpha \frac{\partial}{\partial t}\left(r_\alpha \varepsilon_\alpha\right)+\vec{\nabla}\left[r_\alpha \rho_\alpha \vec{U}_\alpha \varepsilon_\alpha - r_\alpha\left(\mu_\alpha+\frac{\mu_{t\alpha}}{\sigma_\varepsilon}\right)\vec{\nabla}\varepsilon_\alpha\right]=r_\alpha\left[C_1\frac{\varepsilon_\alpha}{k_\alpha}\mu_{t\alpha}\vec{\nabla}\vec{U}_\alpha\left(\vec{\nabla}\vec{U}_\alpha+\left(\vec{\nabla}\vec{U}_\alpha\right)^T\right)-C_2\rho_\alpha\frac{\varepsilon^2}{k}\right] \quad (12)$$

$$\mu_{t\alpha}=\rho_\alpha C_\mu \frac{{k_\alpha}^2}{\varepsilon_\alpha} \quad (13)$$

The present version of the *k-ε* model was named *Asymmetric k-ε turbulence model* by Tamburini et al. (2011a).

Alternatives to specific aspects of the reference modelling approach will be presented later on. In particular alternative inter-phase drag force formulations and different turbulence closures will be tested.

3.2 Modifications to the Inter-phase Drag Force

3.2.1 Dense Particle Effect (DPE)

The Dense Particle Effect (DPE) modification, following Gidaspow (1994), introduces an additional factor E in the inter-phase drag force equation to account for particle-particle interactions in dense suspensions (i.e. high solids loading) so that eq.(6) is rewritten as:

$$\vec{M}_{\alpha\beta} = C_{\alpha\beta}\left(\vec{U}_\beta - \vec{U}_\alpha\right) = \left[\frac{3}{4}\frac{C_{D,turb}^{Brucato}}{d_p} r_\beta \rho_\alpha \left|\vec{U}_\beta - \vec{U}_\alpha\right| E\right]\left(\vec{U}_\beta - \vec{U}_\alpha\right) \tag{14a}$$

where

$$E = \left(1 - r_\beta\right)^{-1.65} \tag{14b}$$

As shown by eq.(14b), larger solid volume fractions lead to an enhancement of the drag force as a consequence of more frequent particle-particle collisions.

3.2.2 Piecewise Correlation (PwC)

This inter-phase drag force modelling was proposed by Tamburini et al. (2009a) and successfully applied for the case of the start-up dynamics of a dense solid-liquid suspension. Three different equations are used for the computation of the inter-phase drag force, each one for a specific solids volumetric fraction range.

- low volumetric fractions ($0 < r_\beta < r_{\beta\_min}$):

  equations 14 are applied, yielding:

$$\vec{M}_{\alpha\beta} = C_{\alpha\beta}\left(\vec{U}_\beta - \vec{U}_\alpha\right) = \left[\frac{3}{4}\frac{C_{D,turb}^{Brucato}}{d_p} r_\beta \rho_\alpha \left|\vec{U}_\beta - \vec{U}_\alpha\right| * \left(1 - r_\beta\right)^{-1.65}\right]\left(\vec{U}_\beta - \vec{U}_\alpha\right) \quad (15a)$$

- high volumetric fractions ($r_{\beta\_\max} < r_\beta < r_{\beta\_packed}$):

  the model adopts the inter-phase force initially proposed by Ergun (1952) to deal with closely packed fixed-bed systems:

$$\vec{M}_{\alpha\beta} = C_{\alpha\beta}\left(\vec{U}_\beta - \vec{U}_\alpha\right) = \left[150\frac{r_\beta^2 \mu_\alpha}{\left(1 - r_\beta\right) d_p^2} + 1.75\frac{r_\beta \rho_\alpha \left|\vec{U}_\beta - \vec{U}_\alpha\right|}{d_p}\right]\left(\vec{U}_\beta - \vec{U}_\alpha\right) \quad (15b)$$

- intermediate volume fractions ($r_{\beta\_\min} < r_\beta < r_{\beta\_max}$):

  for this range a linear interpolation of the two previous equations is used in order to avoid any discontinuity in the $C_{\alpha\beta}$ - r_β relation: this unphysical behaviour would occur if only equations 15a and 15b were employed. Adopting this interpolation with r_{β_min} and r_{β_max} set to 0.35 and 0.45, along with a C_D computed via slip velocity (equation 7), provides in most cases a monotonic dependence of $C_{\alpha\beta}$ *vs* r_β (Tamburini et al., 2009a).

$$\vec{M}_{\alpha\beta} = C_{\alpha\beta}\left(\vec{U}_\beta - \vec{U}_\alpha\right) = \left[C_{\alpha\beta}\left(r_{\beta\_\min}\right) + \frac{C_{\alpha\beta}\left(r_{\beta\_\max}\right) - C_{\alpha\beta}\left(r_{\beta\_\min}\right)}{r_{\beta\_\max} - r_{\beta\_\min}}\left(r_\beta - r_{\beta\_\min}\right)\right]\left(\vec{U}_\beta - \vec{U}_\alpha\right) \quad (15c)$$

3.3 Modification to the turbulence closure

This sub-section is devoted to the description of the modelling approaches which present some modification in the turbulence closure with respect to the *Reference Model*. The turbulence closure concerns both the continuity equations (because of the products between the fluctuating volumetric fractions and the fluctuating velocity components) and the momentum equation (because of the products between the fluctuating velocity components). In the *Reference Model* no turbulence closure is adopted for the continuity equation and, as far as the momentum equation is concerned, only the turbulence closure of the liquid phase is addressed (*asymmetric k-ε turbulence model*).

The *phase specific* treatment, in which k and ε fields are separately computed for each phase, was not taken into consideration in the present study because, as anticipated in the introduction, it involves a greater complexity in the modelling of inter-phase momentum transfer terms and does not offer significant advantages with respect to the homogeneous and the asymmetric models tested here (Montante and Magelli, 2005).

3.3.1 Homogeneous k-ε turbulence model

Momentum equations:

As concerns the modification of the reference momentum equation, both phases are considered here to be turbulent and a turbulent viscosity appears in the momentum equations of both phases. As already mentioned in the introduction the *homogeneous k-ε* turbulence model was found to provide a fair representation of the solid distribution throughout the vessel for a number of cases dealing with dense suspensions in stirred tank (Montante et al., 2001; Micale et al., 2004; Montante and Magelli, 2005; Khopkar et al., 2006; Kasat et al., 2008). Therefore, a *homogeneous k-ε* turbulence model was employed here for comparison purposes with the Reference Model. k and ε transport equations remain practically the same with respect to the single-phase case, but no volume fractions are present and all physical properties appearing in these equations are the "mixture" averaged properties. The interphase drag force formulation is equal to that of the *Reference Model*.

$$\rho_\alpha \frac{\partial\left(r_\alpha \vec{U}_\alpha\right)}{\partial t} + \rho_\alpha \vec{\nabla}\cdot\left(r_\alpha \vec{U}_\alpha \otimes \vec{U}_\alpha\right) = \vec{\nabla}\cdot\left(r_\alpha\left(\mu_\alpha + \mu_{t\alpha}\right)\left(\vec{\nabla}\vec{U}_\alpha + \left(\nabla \vec{U}_\alpha\right)^T\right)\right) - r_\alpha \vec{\nabla} P + r_\alpha \rho_\alpha \vec{g} + \vec{M}_{\alpha\beta} \tag{16}$$

$$\rho_\beta \frac{\partial\left(r_\beta \vec{U}_\alpha\right)}{\partial t} + \rho_\beta \vec{\nabla}\cdot\left(r_\beta \vec{U}_\beta \otimes \vec{U}_\beta\right) = \vec{\nabla}\cdot\left(r_\beta\left(\mu_\alpha + \mu_{t\beta}\right)\left(\vec{\nabla}\vec{U}_\beta + \left(\vec{\nabla} \vec{U}_\beta\right)^T\right)\right) - r_\beta \vec{\nabla} P + r_\beta \rho_\beta \vec{g} - \vec{M}_{\alpha\beta} \tag{17}$$

$$\mu_{t\alpha} = \rho_\alpha C_\mu \frac{k^2}{\varepsilon} \tag{18a}$$

$$\mu_{t\beta} = \rho_\beta C_\mu \frac{k^2}{\varepsilon} \tag{18b}$$

k-ε transport equations:

$$\rho \frac{\partial}{\partial t} k + \vec{\nabla}\left[\rho \vec{U} k - \left(\mu + \frac{\mu_t}{\sigma_k} \right) \vec{\nabla} k \right] = \mu_t \vec{\nabla} \vec{U} \left(\vec{\nabla} \vec{U} + \left(\vec{\nabla} \vec{U} \right)^T \right) - \rho \varepsilon \tag{19}$$

$$\rho \frac{\partial}{\partial t} \varepsilon + \vec{\nabla}\left[\rho \vec{U} k - \left(\mu + \frac{\mu_t}{\sigma_\varepsilon} \right) \vec{\nabla} \varepsilon \right] = C_1 \frac{\varepsilon}{k} \mu_t \vec{\nabla} \vec{U} \left(\vec{\nabla} \vec{U} + \left(\vec{\nabla} \vec{U} \right)^T \right) - C_2 \rho \frac{\varepsilon^2}{k} \tag{20}$$

Velocities and physical properties appearing in equations 19-20 are the "mixture" averaged properties.

$$\rho = r_\alpha \rho_\alpha + r_\beta \rho_\beta \tag{21}$$

$$\vec{U} = \frac{1}{\rho} \left(r_\alpha \rho_\alpha \vec{U}_\alpha + r_\beta \rho_\beta \vec{U}_\beta \right) \tag{22}$$

$$\mu = r_\alpha \mu_\alpha + r_\beta \mu_\beta \tag{23}$$

$$\mu_t = r_\alpha \mu_{t\alpha} + r_\beta \mu_{t\beta} \tag{24}$$

Continuity equations

Turbulence closure may give rise to alternative formulations of the continuity equation (Table 1). In the first and simpler case, the continuity equations are eqs. 1 and 2: the turbulent dispersion of volumetric fractions is neglected (Murthy et al., 2007; Hosseini et al., 2010; Wang et al., 2010; Liu and Barigou, 2013), i.e. the continuity equation does not include the terms arising from Reynolds averaging. Summarizing, this former approach includes turbulence closure terms only in the momentum equations. The *Reference model* case utilizes this approach. When a *homogeneous turbulence model* is used, the neglect of turbulence dispersion terms in the continuity equations gives rise to the treatment called *Homogeneous_no terms* in Table 1.

In a second case, named here *Homogeneous_2 terms*, the *homogeneous model* is used for turbulence and the two continuity equations include additional terms (Zhao et al, 2013):

$$\rho_\alpha \frac{\partial}{\partial t}(r_\alpha) + \rho_\alpha \vec{\nabla} \cdot (r_\alpha \vec{U}_\alpha) - \frac{\mu_{t\alpha}}{\sigma_t} \nabla^2 r_\alpha = 0 \tag{25}$$

$$\rho_\beta \frac{\partial}{\partial t}(r_\beta) + \rho_\beta \vec{\nabla} \cdot (r_\beta \vec{U}_\beta) - \frac{\mu_{t\beta}}{\sigma_t} \nabla^2 r_\beta = 0 \tag{26}$$

where σ_t is a turbulent Schimdt number which is assumed to be equal to 0.8 as suggested by the literature (Montante and Magelli, 2007). According to Montante et al. (2001), contrary to what happens with dynamic phenomena, the sensitivity of the results to this parameter is negligible in steady-state solid-liquid systems. Summarizing, the *Homogeneous_2 terms* approach includes turbulence closure terms in both the continuity and in the momentum equations by means of the homogeneous k-ε model.

Finally a third variant consists of adopting the asymmetric turbulence model and, coherently, in including the dispersion term only in the liquid phase continuity equation (eq. 25), while neglecting it in equation 26 for the solids phase continuity. This approach is dubbed *Asymmetric_1 term* in Table 1. The corresponding results obtained with this approach turned out to be similar to (and actually slightly worse than) those relevant to the *Reference Model* and thus will not be reported in the following for the sake of brevity.

All these variants are relevant to the Reynolds averaging of the governing (continuity and momentum) equation. The Favre averaging is a well-known alternative: in this case, no additional terms arise in the momentum equation while an additional term named turbulent dispersion force has to be included in the momentum equation (Sardeshpande et al., 2011; Gohel et al., 2012). The Reynolds averaging along with the employment of diffusion terms in the continuity equation (to model the product of fluctuating volumetric fraction and the fluctuating velocity) on the one hand

and the Favre averaging along with the inclusion of a suitable turbulence dispersion force in the momentum equation on the other hand, can be considered as just different ways to get consistent results. For this reason, only Reynolds averaged cases are investigated in the present paper.

4 NUMERICAL DETAILS

Central differences were employed for all diffusive terms and the QUICK third-order upwind scheme for the advective ones. The segregated *SIMPLEC* algorithm was adopted to couple pressure and velocity.

Baffles and impeller blades were considered as thin surfaces. No-slip boundary conditions were assumed for all the tank boundaries with the exception of the top surface where free-slip conditions were employed to simulate a free surface.

As far as the treatment of the impeller-baffle relative rotation is concerned, both the steady state Multiple Reference Frame (MRF) by Luo et al. (1994) and the time dependent Sliding Grid (SG) algorithm by Murthy et al. (1994) were adopted in the present work.

Tamburini et al. (2011a) carried out both MRF and SG simulations on system A and found very similar results as regards suspension curves and sediment height. As a consequence, the MRF technique was adopted to simulate the system A in view of its large computational savings.

Conversely, Tamburini et al. (2013b) have shown that different predictions can be found by employing the SG or the MRF approach for the case of system B where local quantities are predicted: as a difference from the suspension curves (integral data) of system A case, the CFD prediction of local solids concentration profiles (data relevant to system B) requires a more accurate calculation, especially if different modelling approaches have to be carefully compared. In accordance with the literature (Ochieng and Lewis, 2006; Panneerselvam et al., 2008) more accurate predictions of the solid-liquid flow field can be provided by the transient SG simulation. Therefore, the transient SG approach was adopted to simulate the system B investigated by

Micheletti et al. (2003). A time step equal to the time the impeller needs to sweep an azimuthal angle equal to a cell (*one cell time step*) was adopted for all the SG simulations performed.

The position of both the surface separating the two domains both in the SG and in the MRF framework was chosen in accordance with the assumptions of Luo et al. (1994) at the dimensionless radial position R = 0.62 (T/2).

According to the systems axial symmetry, only one half of the tank was included in the computational domain and two periodic boundaries were imposed along the azimuthal direction. The structured grid chosen for the discretization of system A encompasses 53760 cells distributed as 24 × 70 × 32 along the azimuthal, axial and radial direction, respectively. The computational grid is finer in the proximity of the impeller where the largest gradients of the flow variables are expected. A similar structured grid with 74592 computational cells (distributed as 72 × 37 × 28 along the axial, radial and azimuthal direction respectively) was employed for system B of Micheletti et al. (1994). As well-known in the literature, the choice of adopting a completely hexahedral grid may allow, for any given required accuracy, a discretization degree much lower than that necessary for a tetrahedral discretization of the computational domain (Scully and Frawley, 2011; Tamburini et al., 2012d).

In order to assess the grid dependence of the CFD results, Tamburini et al. (2011a) and Tamburini (2011) employed computational grids up to 8 times finer for the two systems and found no significant grid dependence. In particular the mean value of the discrepancy between the finest grid and the grid adopted here was found to be ~1.0% for r_β which is the most significant variable in solid-liquid systems. Therefore, only coarse grid simulations were performed for the purpose of the present work in view of its comparative nature and of the large number of test cases investigated.

The *Excess Solid Volume Fraction Correction* (ESVC) algorithm firstly proposed by Tamburini et al. (2009a) and successively optimized by Tamburini et al. (2011a) was adopted since partial suspension conditions were investigated in the present work. This algorithm guarantees that the maximum packing volumetric fraction r_{β_packed} is not exceeded in the computational domain even at

very low impeller speeds, when a sediment is present. It operates iteratively at the end of each SIMPLEC iteration forcing the volumetric fractions exceeding r_{β_packed} (*solid-excess*) to be distributed among the neighbouring computational cells and eventually moved towards regions where no solid-excess is present.

The *Unsuspended Solid Criterion* (USC) proposed by Tamburini et al. (2011a) was employed to compute the mass fraction of suspended particles. In accordance with this criterion solid particles are judged as being unsuspended if and only if they belong to cells where $r_\beta \geq r_{\beta\_packed}$.

Both these algorithms were found suitable to deal with solid-liquid suspensions in baffled stirred tank under partial to complete suspension regimes (Tamburini et al., 2011a, 2012a,b and 2013b).

Typically in MRF steady state simulations 12000 SIMPLEC iterations were found to be sufficient for variable residuals to settle to very low values in all the investigated cases and to allow the *ESVC* algorithm to efficiently operate.

As concerns the time dependent SG simulations of system B, 100 full revolutions were found sufficient to reach steady state conditions, in agreement with the literature (Micale et al., 2004; Tamburini et al., 2009a, 2011a, 2013b,c). The number of SIMPLEC iterations per time step was set to 30 to allow residuals to settle before moving to the next time step.

As far as the initial guess or initial condition is concerned, the fluid was assumed to be still and the particles were considered to be motionless on the vessel bottom and at their maximum packing value r_{β_packed}.

5 RESULTS AND DISCUSSION

5.1 Results of the *Reference Model*

The comparison between the experimental values relevant to system A and system B and the corresponding CFD predictions provided by the *Reference Model* are shown in the following

Figures 2 and 3. Experimental data include the suspension curves and the normalized sediment height as visually observed on the lateral wall midway two subsequent baffles for the case of system A and local axial profiles of solid concentration for the case of system B.

As far as the suspension phenomenon is concerned, the discrepancy between the experimental and the CFD data relevant to system A is acceptable. The suspension curves are shown in Fig.2a where some overestimations of the experimental data can be observed, especially for the case of the largest particles. Only for the case of the low-concentration/small-particles case a slight underestimation is found at about 250-300rpm.

The sediment height is another feature of the suspension phenomenon and is reported in Fig.2b. In this case a very good agreement is found: only slight differences can be observed.

As it concerns the prediction of the particle distribution phenomenon, the prediction of the experimental local axial profiles of solid concentration via the *Reference Model* for system B is reported in Fig.3: each profile is relevant to a specific impeller speed ranging from highly incomplete (i.e. 400rpm) to complete (i.e. 1100rpm > N_{js}) suspension conditions. All the experimental profiles are satisfactorily followed by the CFD data, although the particle distribution degree is slightly underestimated. More precisely, at 400rpm and 500rpm the experimental data at the very top of the vessel are not perfectly matched by the CFD predictions; while a somewhat larger discrepancy can be observed below the impeller at impeller speeds of 600rpm and 700rpm.

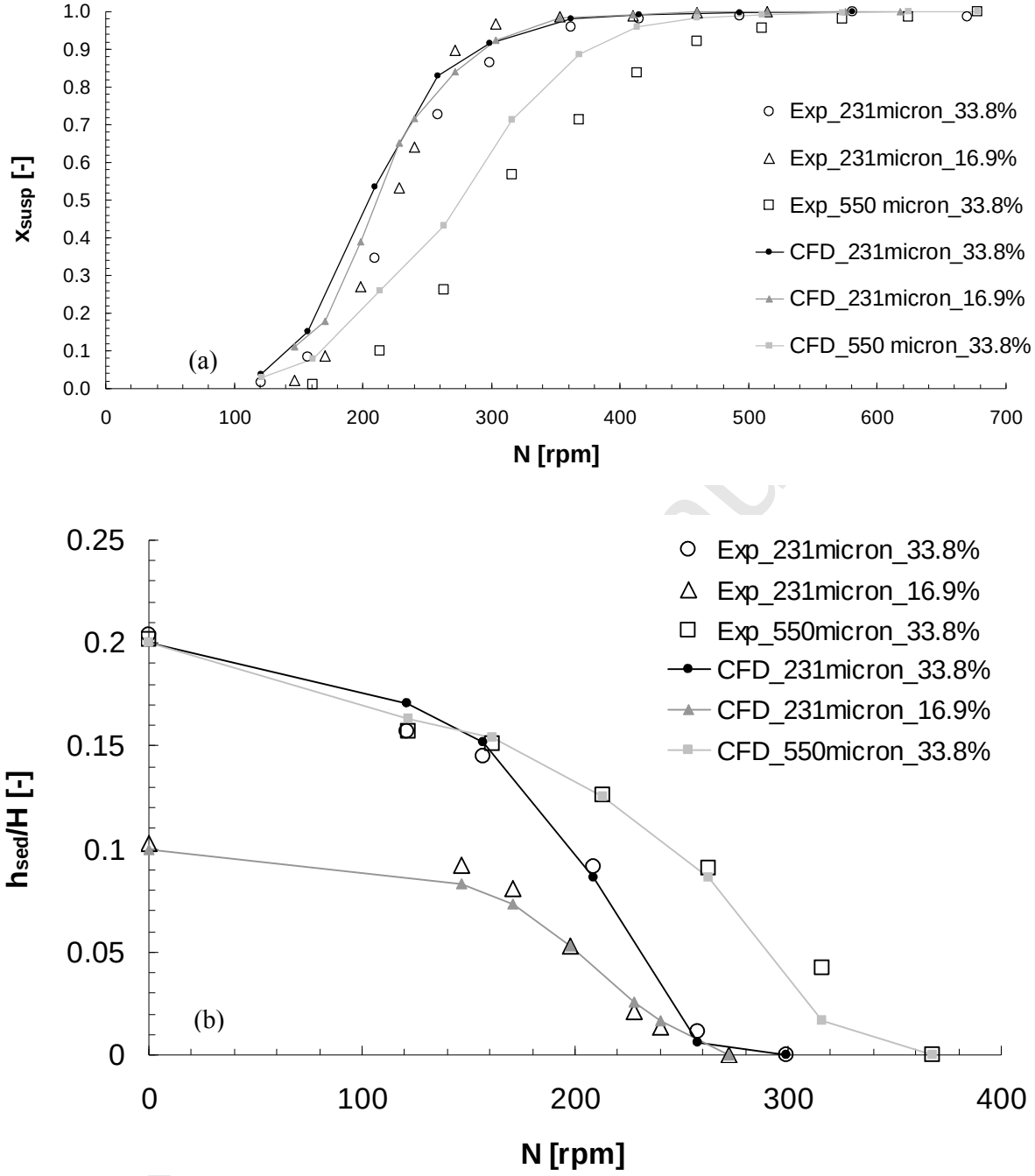

Fig. 2: Reference Model MRF simulations versus experimental data (Tamburini et al., 2011a) for system A. (a) suspension curves, (b) normalized sediment heights.

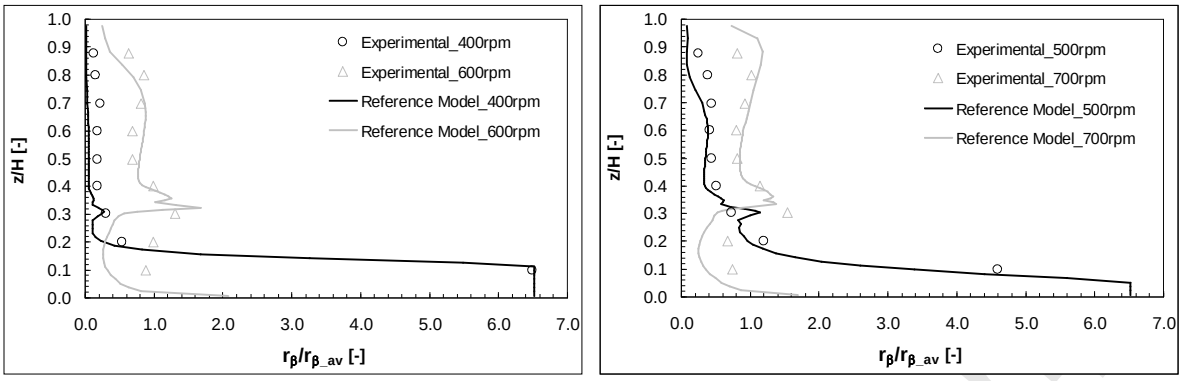

Fig. 3: Local axial profiles of solid concentration (system B): Reference Model SG simulations versus experimental data (Micheletti et al., 2003).

Summarizing, all the experimental data are fairly well predicted by the very simple *Reference Model*, although there seems to be still room for further improvements. In the following, some modifications to the present *Reference Model* will be tested with the aim at improving the predictions of the experimental data. Therefore, in the following the discussion will be focused on the influence of the modelling modifications described in section 3 (concerning inter-phase drag force and turbulence closure) on the prediction of the experimental data.

5.2 Influence of model changes – System A

5.2.1 Interphase Drag Force modelling

Suspension Curves

As it can be seen in Fig.4, neither of the proposed modifications to the interphase drag force provides satisfactory results: both of them significantly overestimate the experimental data as well as the predictions of the *Reference Model*, especially at the intermediate impeller speeds. The present modifications appear to lead to a premature suspension of a large amount of solid particles. However, both the *Dense Particle Effect* approach and the *Piecewise Correlation* approach are able to predict the typical sigmoidal trend of the suspension curve.

As regards the *DPE* approach, the drag force enhancement due to the dense particle effect may cause an overestimation of the momentum exchange between phases thus providing a suspended solid fraction higher than the experimental one. The higher the local r_β, the higher the influence of the dense particle effect term, so one may expect a larger influence at low N when the particle distribution degree is very small. Actually, when particles are lying packed on the bottom as sediment they show the same $r_\beta = r_{\beta\text{-}packed}$, so that the drag force enhancement is the same in all cells where sediment is present, independently of the impeller speed.

When the impeller speed is very low, the drag force is not sufficient to suspend many particles (even if the *DPE* enhancement is accounted for) because the slip velocity between the liquid flow and the sediment is still too low. As the agitation speed increases, the slip velocity increases (the liquid velocity increases, while the solids velocity remains still low) and the drag force reaches its critical value for the suspension of a large fraction of particles (i.e. when the curve starts to rise with a large slope). In general, when a *DPE* approach is employed the drag force reaches its critical value at impeller speeds lower than those of the *Reference Model*, thus yielding an overestimation of the amount of suspended particles.

As far as the *Piecewise Correlation* (*PwC)* approach is concerned, Fig.4 shows that at very low impeller speeds the mass fractions of suspended solids predicted by the *PwC* and *DPE* methods are very similar thus suggesting that even the increase of the drag force induced by the adoption of the Ergun equation is not sufficient to allow particles to suspend when the slip velocity is low. At higher impeller speeds the over-prediction provided by the *PwC* approach appears to be similar and slightly larger than that of the *DPE* model.

This behaviour is confirmed by Fig.5 where the comparison of the same approaches is presented for the case of a solid-liquid suspension with the same geometry and particle size, but a lower solids loading. The Ergun equation provides a larger increasing of the interphase drag force thus leading to x_{susp} values higher than those predicted by the *DPE* approach.

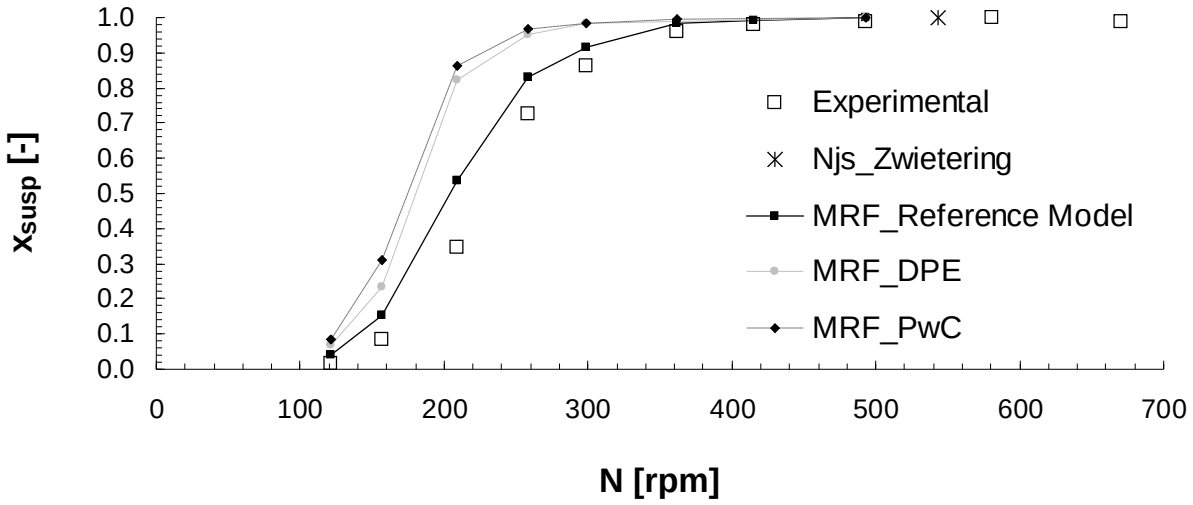

Fig. 4: MRF simulations versus suspension curve experimental data (Tamburini et al., 2011a) for the case of 212-250 μm glass ballottini particles with a solid loading of 33.8%$^{w/w}$: comparison of different drag force formulations.

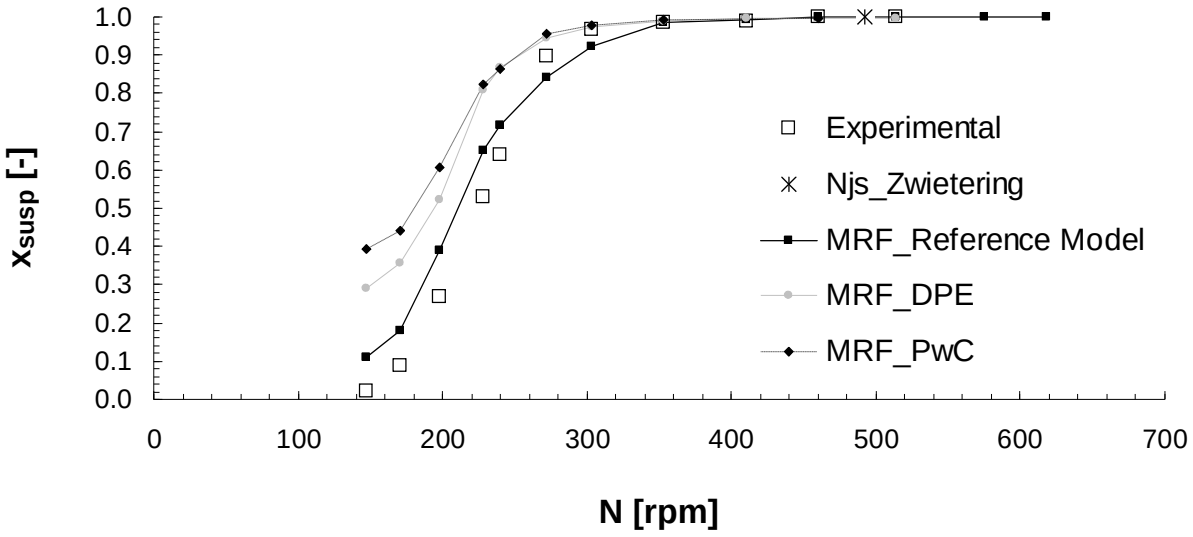

Fig. 5: MRF simulations versus suspension curve experimental data (Tamburini et al., 2011a) for the case of 212-250 μm glass ballottini particles with a solid loading of 16.9%$^{w/w}$: comparison of different drag force formulations.

As a difference with the previous case, here a large overestimate of the experimental data is observed for the two alternative approaches even at the lowest impeller speeds. The predictions of Hosseini et al. (2010) concerning cloud height and homogenization degree show a similar overestimate at the lower impeller speeds for a similar solids loading (10%$^{w/w}$). By a close

inspection of Figs 4 and 5 it is possible to note that at, for example, 150rpm the x_{susp} values predicted by the *DPE* and the *PwC* approaches for the case of the more diluted suspension (Fig.5) are about twice those predicted for the case with the larger solids loading (Fig.4). Independently of the solids loading, when the impeller speed is very low, particles are packed over the bottom exhibiting the maximum allowed volume fraction as well as the same particle-particle interactions. As a consequence the *DPE* approach on the one hand, and the *PwC* approach on the other hand, produce drag force enhancements which remain constant with the solids loading thus predicting a similar quantity of particles to be suspended. For the more dilute suspension this quantity corresponds to a larger fraction of suspended particles.

At higher impeller speeds, no differences between the x_{susp} values predicted by the *DPE* and the *PwC* approaches are appreciable. This occurrence is not surprising as for moderate solids loadings, when most particles are suspended throughout the vessel, r_β is relatively low. As a consequence, the *PwC* approach switches to equation 15a, thus yielding drag force predictions identical to the *DPE* approach.

As it is shown in Fig.6, the two approaches provide over-predictions larger than those of the *Reference Model* also for the case of the solid-liquid suspension with larger particle size thus confirming that taking into account the particle-particle interactions via the proposed drag force modifications is not suitable for partial suspension conditions.

As concerns the comparison between the *DPE* and the *PwC* approaches, Fig.6 shows that they provide practically identical results thus suggesting that for the present case the Ergun equation and the Gidaspow correction produce the same increment of the inter-phase drag force. This difference with respect to the previous cases (where different increments were found) may be linked to the presence of the Brucato et al drag-turbulence correlation (1998) whose effect is negligible for the lower particle diameter case as it can be seen in Tab.2. In accordance with this correlation, the higher the particle diameter, the higher the enhancement of the drag coefficient. This correction does not appear in the Ergun equation, thus suggesting that the gap in drag force predictions

between the two approaches for the lower particle size cases may be bridged by the action of the drag coefficient enhancement due to the liquid free stream turbulence. This hypothesis might be confirmed by observing in Fig.6 that at 368rpm and 413rpm the *DPE* approach yields x_{susp} slightly larger than those by *PwC* approach since the higher the impeller speed, the lower the Kolmogorov length scale λ, the higher the drag coefficient enhancement.

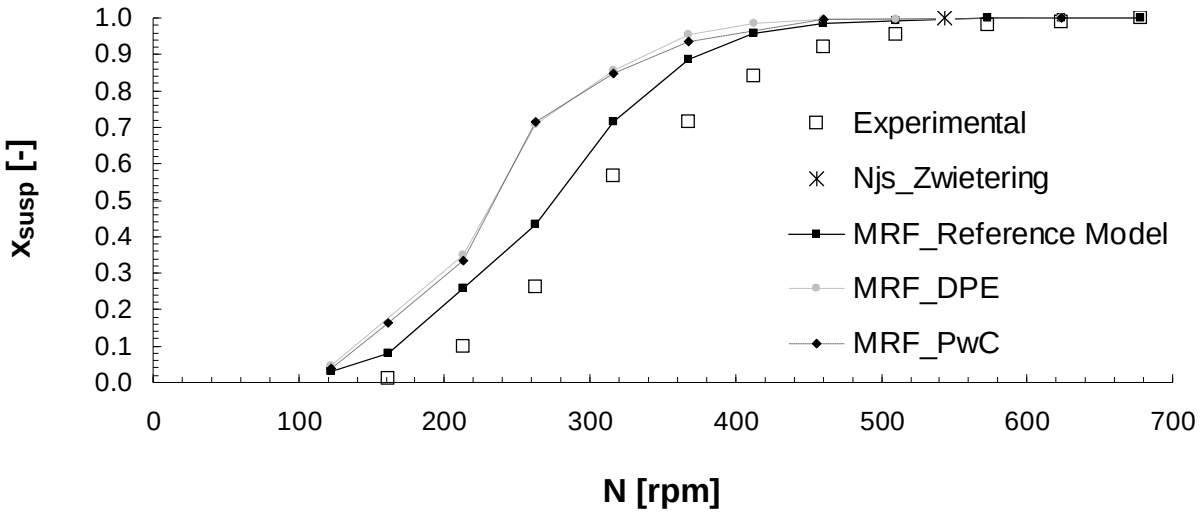

Fig. 6: MRF simulations versus suspension curve experimental data (Tamburini et al., 2011a) for the case of 500-600 μm glass ballottini particles with a solid loading of 33.8%$^{w/w}$: comparison of different drag force formulations.

Sediment Height

The following Figs 7,8 and 9 show the normalized sediment height for the same configurations for which Figs 4,5 and 6 report suspension curves. Notably, the sediment height data represent only a local piece of information and should be regarded as less decisive for comparison purposes than the more global information provided by the suspension curves.

By observing Fig.7 (small particles, higher solids loading) considerations similar to those presented in the former sub-section for Fig.4 can be made. Both the *DPE* and the *PwC* approaches yield an underestimation of both the experimental data and the CFD predictions obtained by the *Reference Model*. Also, *PwC* yields larger underestimations than *DPE*.

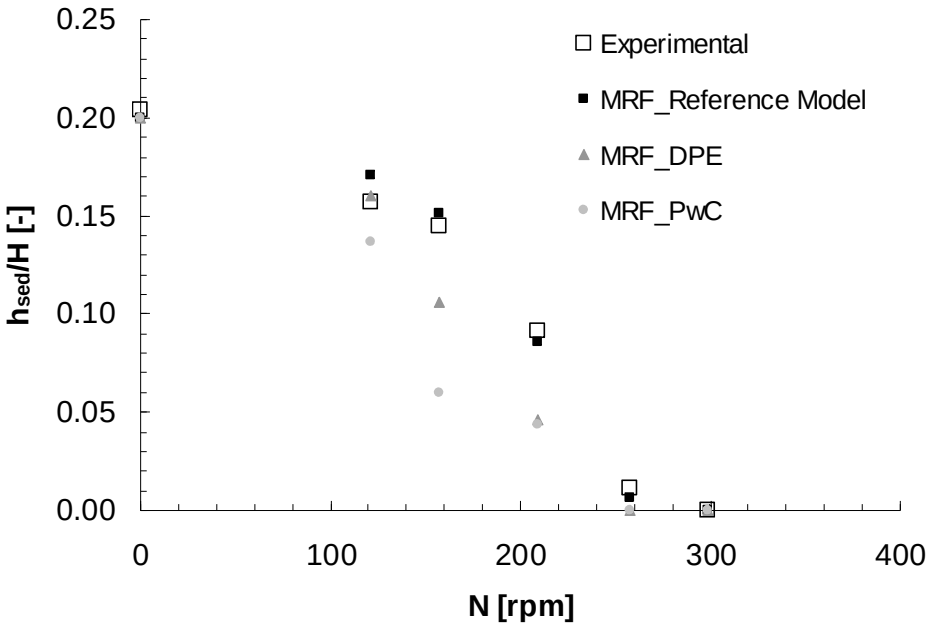

Fig. 7: MRF simulations versus sediment height experimental data (Tamburini et al., 2011a) for the case of 212-250 μm glass ballottini particles with a solid loading of 33.8%$^{w/w}$: comparison of different drag force formulations.

In Fig.8 (small particles, lower solids loading) a surprisingly different behaviour can be observed: as a difference with the corresponding suspension curve results in Fig.5, here all the approaches yield very similar results and predict values of h_{sed} in good agreement with the experiments.

This occurrence can be explained by considering the 3D visualization of the sediment estimated by the simulations, shown in Fig.9. Here the computational cells where $r_\beta \geq r_{\beta\_packed}$ (sediment) are indicated in grey. Contours of the solids volumetric fraction on a vertical diametrical plane are also reported. The *DPE* and the *PwC* results exhibit a sediment distribution along the peripheral wall (and thus a h_{sed} value) similar to the reference case, but differ in the way sediment is suspended from the central region of the tank bottom (and thus in the x_{susp} value).

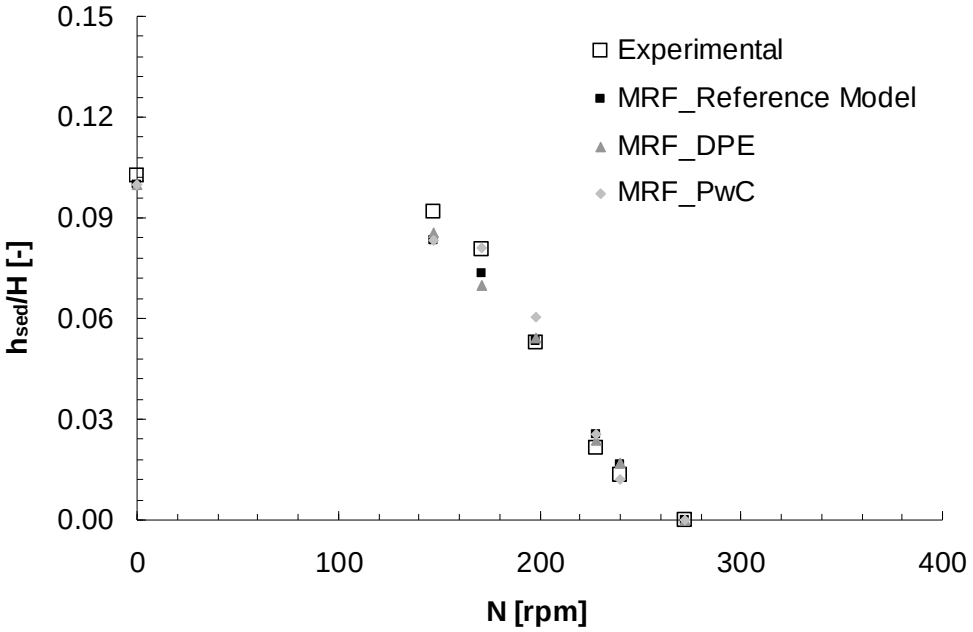

Fig. 8: MRF simulations versus sediment height experimental data (Tamburini et al., 2011a) for the case of 212-250 μm glass ballottini particles with a solid loading of 16.9%$^{w/w}$: comparison of different drag force formulations.

The impeller speed of 171rpm showed in Fig.9 is just an example: the same behaviour is also observable at 125rpm and 147rpm. Such behaviour is not in accordance with the extensively validated *Reference Model* results and with experimental visualization (Tamburini, 2011) where particles seem to suspend preferentially from the peripheral region of the sediment. Conversely, the analysis of the 3-D sediment visualization for the other two suspension cases showed that the three model approaches predict similar sediment shape evolution as a function of the impeller speed. Clearly, a feature like the shape of the sediment is the result of a delicate balance among different forces including pressure gradients, drag and turbulent stresses so that it is not surprising that even slight model changes may results in significant differences in the predictions.

Fig.10 (large particles, high solids loading) is perfectly in accordance with the corresponding Fig.6: the *DPE* and the *PwC* approaches provide the same under-predictions of the experiments and of the data obtained by applying the *Reference Model*.

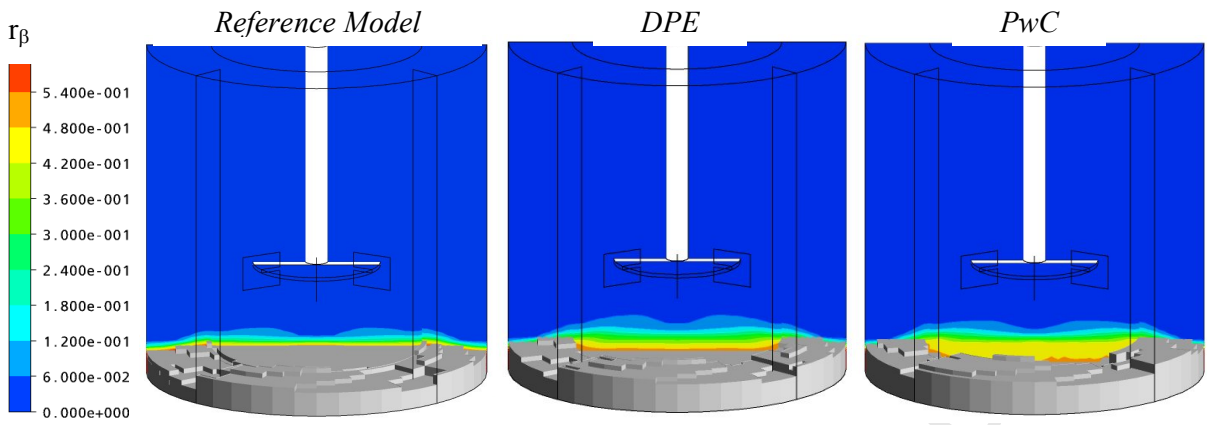

Fig. 9: 3-D sediment visualization plot upon contour plots of solid volumetric fractions on a vertical diametrical plane at 171rpm for the case of 231 μm ballottini particles at 16.9%$^{w/w}$: comparison of different drag force formulations

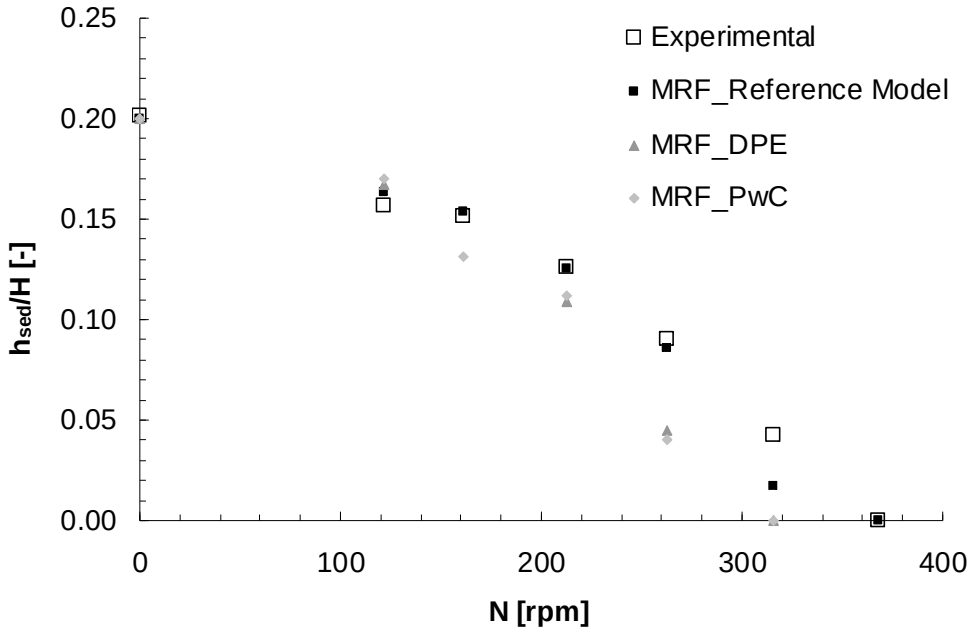

Fig. 10: MRF simulations versus sediment height experimental data (Tamburini et al., 2011a) for the case of 500-600 μm glass ballottini particles with a solid loading of 33.8%$^{w/w}$: comparison of different drag force formulations.

5.2.2 Turbulence closure

Suspension Curves

Fig.11 reports experimental and computational results concerning the suspension curves for system A with small particles and high solids loading. The adoption of the homogeneous *k-ε* turbulence

model along with no additional terms in the continuity equation (*Homogeneous_no terms*) provides results which are similar to those obtained by the *Reference Model*, even closer to the experimental data at the intermediate impeller speeds. The reason of this finding is closely related to the homogeneous k-ε turbulence model fundamentals. The two phases share the same turbulence kinetic energy k and the same dissipation of turbulence kinetic energy ε which are calculated by employing the mixture quantities. At low to intermediate impeller speeds, when a sediment is present, the mixture velocity used by the turbulence model near the sediment-fluid interface results to be quite lower than that of the liquid phase, thereby leading to compute small velocity gradients, smaller turbulence productions and thus a less intensive turbulence. This fact causes the suspension of a quantity of particles lower than that of the *Reference Model*.

As a difference, when the additional terms are included in the continuity equation (*Homogeneous_2 terms*), very large overestimation of x_{susp} are obtained, even at very low impeller speeds (Fig.11). This occurrence is linked to the nature of the additional terms including the Laplacian of the volumetric fraction. The action of such term is particularly strong at the sediments interface and results in making this interface a diffuse one from which solid particles are more easily dragged by the liquid.

In accordance with Mersmann et al. (1998) the suspension of solid particles is strictly linked to two different phenomena: the *bottom lifting* and the *avoidance of settling*. Which of them may be the one controlling the particle suspension depends on particle and liquid properties, on solids hold up, on impeller to tank diameter ratio. By applying the "*decisive criterion for suspension*" by Mersmann et al. (1998) (see following eq.27) it results that bottom lifting is the phenomenon controlling the solid suspension for all the cases investigated in the present work, i.e. the amount of energy necessary to allow the particles to lift from the tank bottom $\overline{\varepsilon_{BL}}$ is higher than that necessary to avoid the suspended particles to settling $\overline{\varepsilon_{AS}}$ (the ratio of eq.27 results higher than 1 for all the cases studied here):

$$\frac{\overline{\varepsilon_{BL}}}{\varepsilon_{AS}} \approx 527\left(\frac{T}{D}\right)^{5/2}\frac{d_p}{H}\frac{1}{Ar^{1/8}\left[r_{\beta\_av}\left(1-r_{\beta\_av}\right)^n\right]^{1/4}} \tag{27}$$

where *Ar* is Archimedes number and *n* is an exponent depending on the value of *Ar*. Full details can be found in the work by Mersmann et al. (1998).

The inclusion of the additional terms in the continuity equation largely aids the bottom lifting phenomenon thus allowing a large amount of particles to be prematurely suspended.

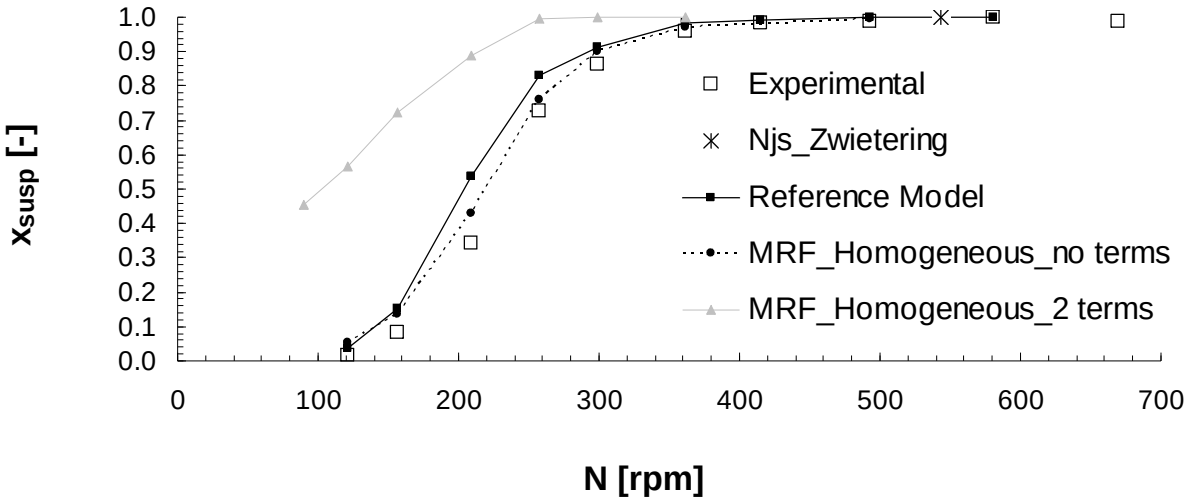

Fig. 11: MRF simulations versus suspension curve experimental data (Tamburini et al., 2011a) for the case of 212-250 μm glass ballottini particles with a solid loading of 33.8%$^{w/w}$: comparison of different turbulence closures.

The relative effectiveness of alternative approaches appears to be quite independent of particle concentration and mean diameter. By observing Figs. 12 (small particles, low solids loading) and 11 (large particles, high solids loading) considerations similar to those relevant to Fig.11 can be made: the x_{susp} values predicted by the *Homogeneous_no terms* approach are lower than those obtained by the *Reference Model* and generally closer to the experimental data. Conversely the adoption of the *Homogeneous_2 terms* approach gives rise for both suspensions to over-predictions at all the impeller speeds and particularly at low speeds. This results is in agreement with the findings by Fletcher and Brown (2009) who found that the *homogeneous* and the *asymmetric k-ε* models

provide similar results, but the homogeneous model leads to a lower particle dispersion. They stated also that the inclusion of turbulent dispersion (as done in the case of *Homogeneous_2 terms* approach) leads to a great enhancement of particle dispersion and that the soundness of its adoption at low impeller speeds has to be carefully validated.

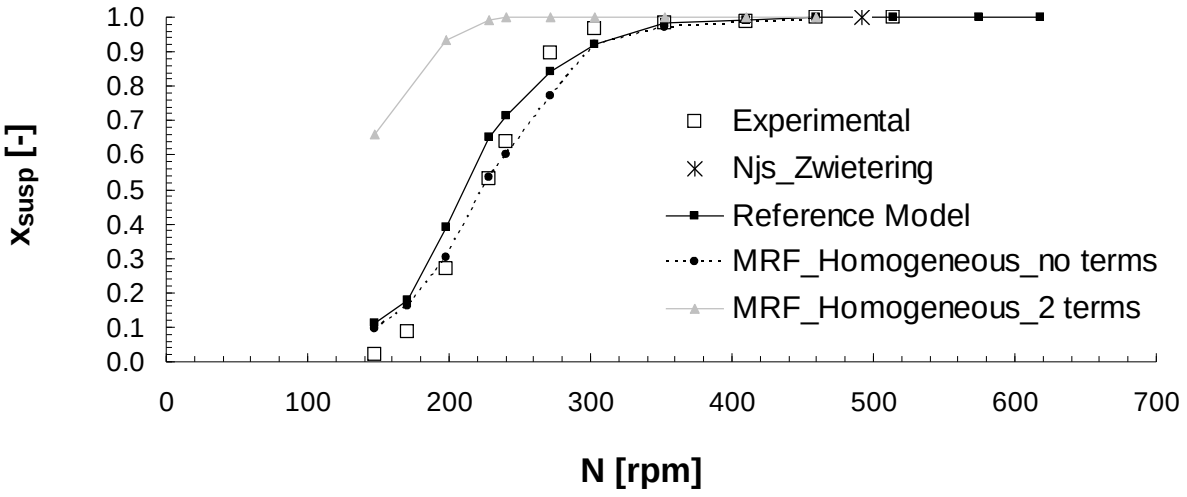

Fig. 12: MRF simulations versus suspension curve experimental data (Tamburini et al., 2011a) for the case of 212-250 μm glass ballottini particles with a solid loading of 16.9%$^{w/w}$: comparison of different turbulence closures.

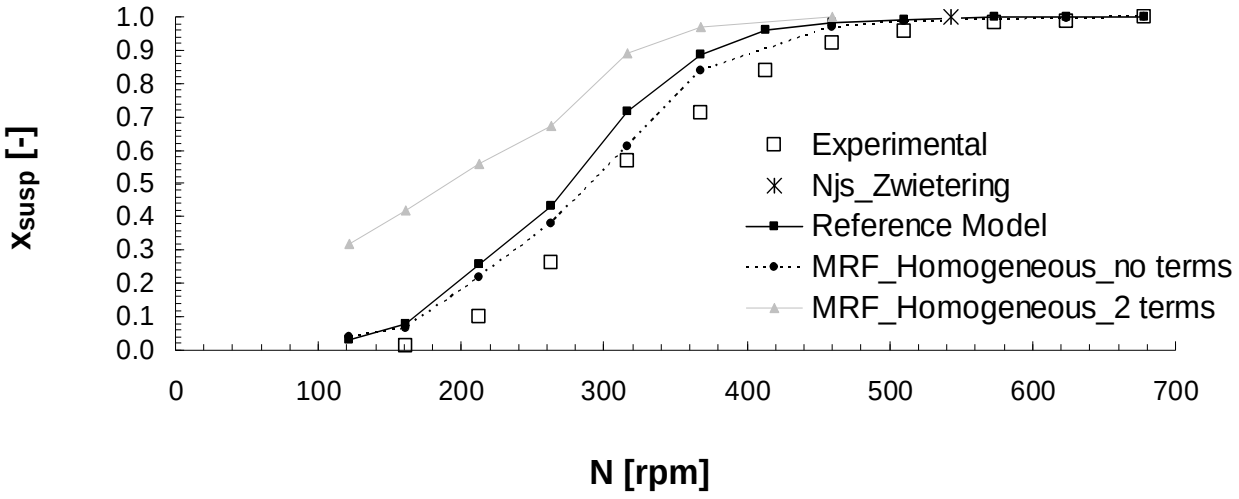

Fig. 13: MRF simulations versus suspension curve experimental data (Tamburini et al., 2011a) for the case of 500-600 μm glass ballottini particles with a solid loading of 33.8%$^{w/w}$: comparison of different turbulence closures.

Sediment Height

In Fig.14 the comparison of the sediment heights provided by the different turbulence closures for the case of 212-250 μm glass ballottini particles with a solid loading of 33.8%$^{w/w}$ is shown. The *Reference Model* and the *Homogeneous_no terms* predictions appear to be quite similar and in a good agreement with the experimental data.

The *Homogeneous_2 terms* approach provides very low h_{sed} values. This result is in accordance with the large underestimation of the amount of unsuspended particles presented in Fig.11.

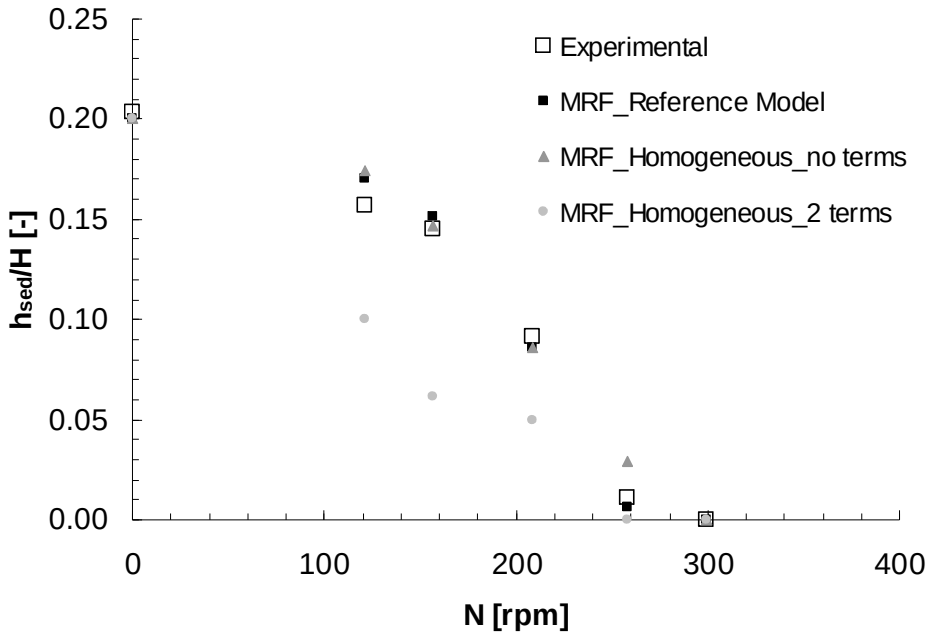

Fig. 14: MRF simulations versus sediment height experimental data (Tamburini et al., 2011a) for the case of 212-250 μm glass ballottini particles with a solid loading of 33.8%$^{w/w}$: comparison of different turbulence closures.

As concerns the small particle, low solids loading case, Fig.15, by comparing the predictions of the *Reference Model* and the *Homogeneous_no terms*, it appears that these are very similar only for impeller speeds lower than 180rpm. This is in accordance with the results shown in Fig.12, where similar x_{susp} values can be observed for the two approaches in the same impeller speed range. As a

difference with Fig.12, at impeller speeds higher than 180rpm, the *Reference Model* predictions are closer to the experimental data than the *Homogeneous_no terms* ones.

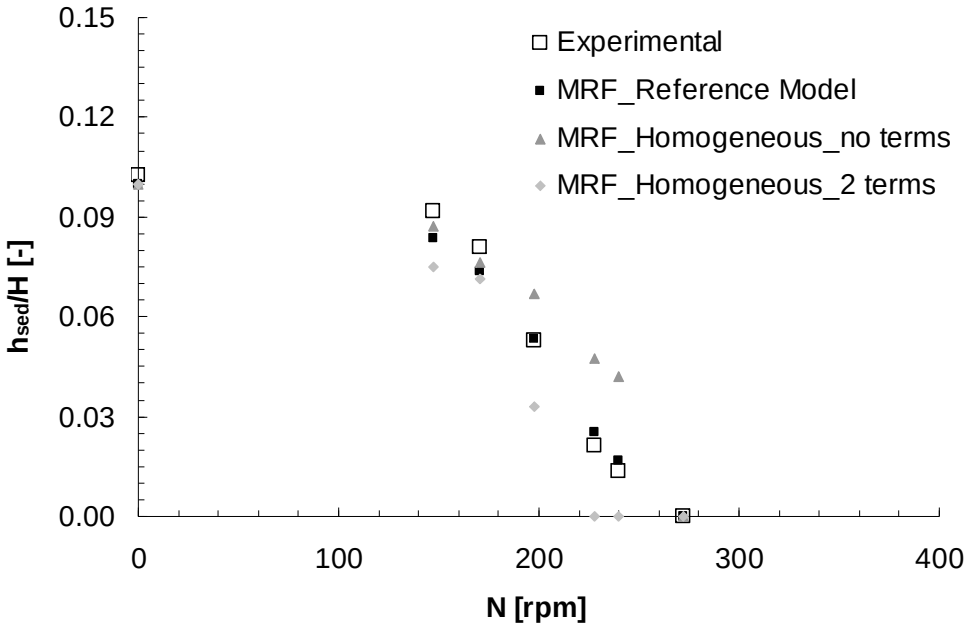

Fig. 15: MRF simulations versus sediment height experimental data (Tamburini et al., 2011a) for the case of 212-250 μm glass ballottini particles with a solid loading of 16.9%$^{w/w}$: comparison of different turbulence closures.

The *Homogeneous_2 terms* approach leads to h_{sed} values lower than the experiments and the other predictions. At 147rpm and 171rpm the discrepancies between the *Homogeneous_2 terms* and the relevant experimental h_{sed} are lower than the corresponding discrepancies between the x_{susp} values observable in Fig.12. The use of *Homogeneous_2 terms* approach results into the suspension of most particles from the bottom centre (Fig.16), in a similar way as previously shown in Fig.9 for the influence of the drag model in Section 5.2.1, thus providing largely different x_{susp} at similar h_{sed}. As already stated for the cases of the *DPE* and *PwC* approaches, the vigorous suspension from the bottom centre is not consistent with the experimental evidence for a T/2 Rushton turbine thus suggesting that the *Homogeneous_2 terms* is not suitable to deal with the case under study.

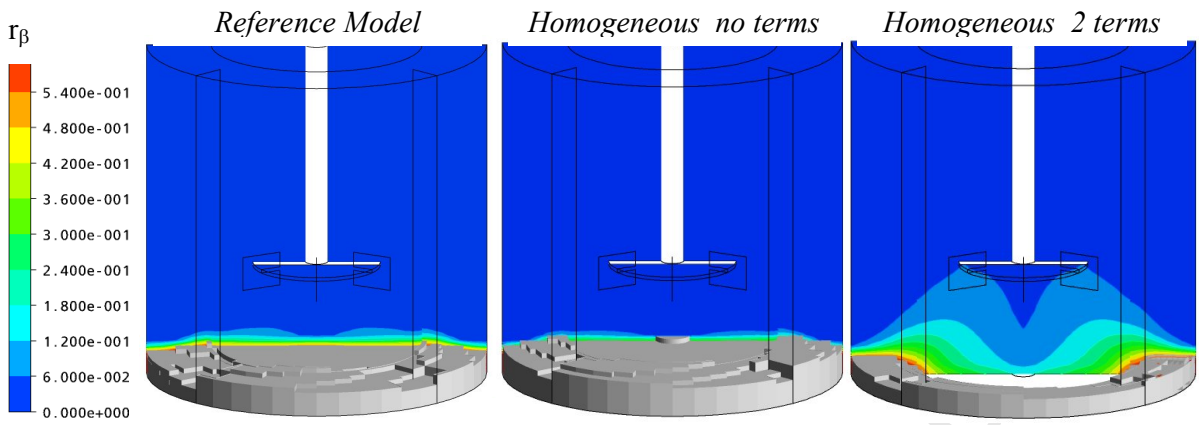

Fig. 16: 3-D sediment visualization plot upon contour plots of solid volumetric fractions on a vertical diametrical plane at 171rpm for the case of 231 μm ballottini particles at 16.9%$^{w/w}$: comparison of different turbulence closures

As far as the case of a suspension with large particle size is concerned, the comparison among the different modelling approaches is shown in Fig.17.

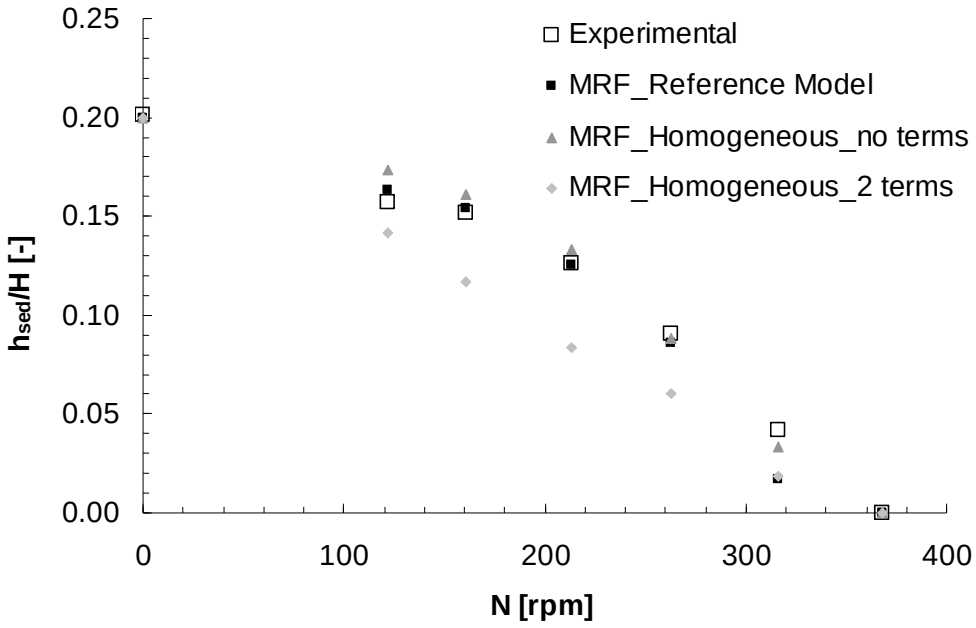

Fig. 17: MRF simulations versus sediment height experimental data (Tamburini et al., 2011a) for the case of 500-600 μm glass ballottini particles with a solid loading of 33.8%$^{w/w}$: comparison of different turbulence closures.

These results are coherent with the corresponding ones for the suspension curve depicted in Fig.13: the *Homogeneous_no terms* provides the highest h_{sed} values and the lowest x_{susp} values, on the contrary, the *Homogeneous_2 terms* provides the lowest h_{sed} and the largest x_{susp} values.

Summarizing, both the *Reference Model* and the *Homogeneous_no terms* approach are able to provide satisfactory predictions of the normalized sediment height. Particularly, the *Reference Model* predictions generally appear better than those obtained with the *Homogeneous_no terms* approach. Finally, the inclusion of the turbulence closure additional terms in the continuity equations gives rise to a very large underestimation of the h_{sed} values thus suggesting that the *Homogeneous_2 terms* approach may be unsuitable to manage suspension phenomena in solid-liquid agitated systems operated under medium-to-highly incomplete suspension conditions.

5.3 Influence of model changes - System B

The experimental data employed so far for quantitative validation purposes are relevant to the amount of solid particles lying on the vessel walls (bottom and lateral wall), but they do not provide a quantitative description of the particle distribution over the vessel.

Therefore, local axial profiles of solid concentrations for a similar system (the system B by Micheletti et al., 2003) were selected from the literature for a further comparison of the different modelling approaches.

5.3.1 Interphase Drag Force modelling

Fig. 18 reports sliding grid (SG) predictions and experimental results for the profiles for five different impeller speeds. It should be observed that SG results are intrinsically time-dependent ones, however, at a radial location sufficiently away from the impeller tip (as in the present case where data refer to R=0.35T, while the outer impeller tip is at R=0.16T) results are practically time-independent so that instantaneous results are practically coincident with the time-averaged ones.

When the slip velocity between the two phases is still too low as in the case at 400rpm, accounting for the particle-particle interactions in the drag force formulation does not provide any significant difference: as a matter of fact Fig. 18 shows that at this impeller speed the predicted axial profiles of r_β are very similar. This is in accordance with the results shown in Section 5.2.1, e.g. Fig. 4, for the case of system A: when the slip velocity between the two phases is still too low, enhancements of the drag force do not produce the suspension of the particles which remain on the bottom thus showing a negligible axial dispersion degree.

As a difference, at 500rpm, the increased slip velocity along with the particle-particle interaction effects cause an excessive degree of suspension to be predicted. Although both the *DPE* and *PwC* approaches predictions are not far from the experimental data at intermediate heights, they do not succeed in predicting the amount of particles placed in the proximity of the vessel bottom, where the drag force enhancement provided by both approaches lead to an excessive particle suspension. These two approaches show some difference between each other in the lower part of the tank allegedly because of Ergun's equation effect which is a peculiarity of the *PwC* approach.

At 600rpm all the approaches provide the same results up to z/H = 0.7, showing the same underestimation of the experimental data. As far as the upper part of the vessel is concerned (z/H > 0.7) the adoption of Gidaspow's correction (*DPE* and *PwC*) seems to generate a better agreement with the experimental data than the *Reference Model*. Note that at these low r_β the *DPE* and the *PwC* approaches practically reduce to the same eq. 15a.

At higher impeller speed (i.e. 700rpm and 1100rpm) the particles are better distributed throughout the vessel thus leading to a r_β value close to the r_{β_av} in almost all computational cells. In these conditions, the drag force enhancement produces by the *DPE* and the *PwC* approaches appears practically not to affect the particle distribution.

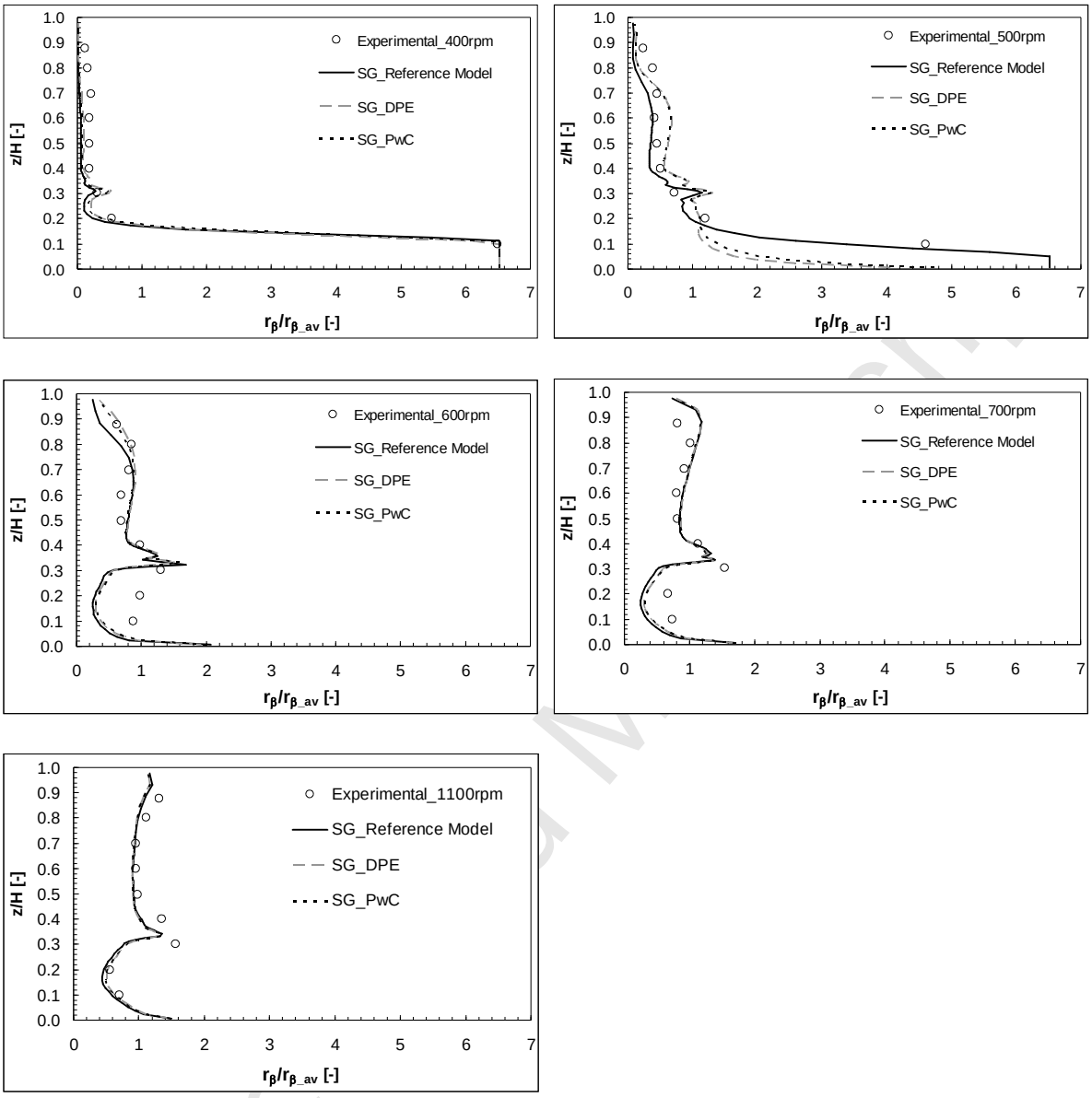

Fig. 18: SG simulations versus steady state local axial profiles of particle concentrations (midway between subsequent baffles and at R = 0.35T) at different impeller speeds for the case of 600-710 μm glass ballottini particles with a solid loading of 25%$^{w/w}$: comparison of different drag force formulations. Experiments were collected by Micheletti et al. (2003).

5.3.2 Turbulence closure

As it can be seen in Fig.19, at 400rpm the results provided by the *Reference Model* and the *Homogeneous_no terms* approach are practically identical and in a good agreement with the

experimental data. Conversely, the inclusion of the additional turbulence-based terms in the continuity equation leads to an excessive suspension coherent with the premature particle suspension shown by the suspension curves results for system A using the same approach, Figs. 11-13 as already discussed for the suspension curves for the case of system A.

At 500 rpm the *Homogeneous_2 terms* approach causes a dramatic overestimation of the particle distribution degree. The *Homogeneous_no terms* approach behaves slightly better than the *Reference Model* in the lowest part of the vessel, while it appears slightly worse in the upper part.

At 600rpm and 700rpm, unlike the *Reference Model* and the *Homogeneous_no terms* approach predictions, the *Homogeneous_2 terms* approach does not underestimate the r_β experimental values below the impeller plane, while it under-predicts the peak of the experimental profile near the impeller mid-plane. Also in these cases the results of the *Reference Model* and of the *Homogeneous_no terms* approach are very similar: the only significant differences concern the upper region of the vessel, where the *Reference Model* predictions are closer to the experiments at 600rpm, while the *Homogeneous_no terms* approach results are in better agreement with the experiments at 700rpm.

At 1100 rpm, under complete suspension conditions, the *Reference Model* and the *Homogeneous_no terms* approach provide the same predictions which follow well the experimental profile. The *Homogeneous_2 terms* predictions, being closer to homogeneous conditions, are further from the experiments.

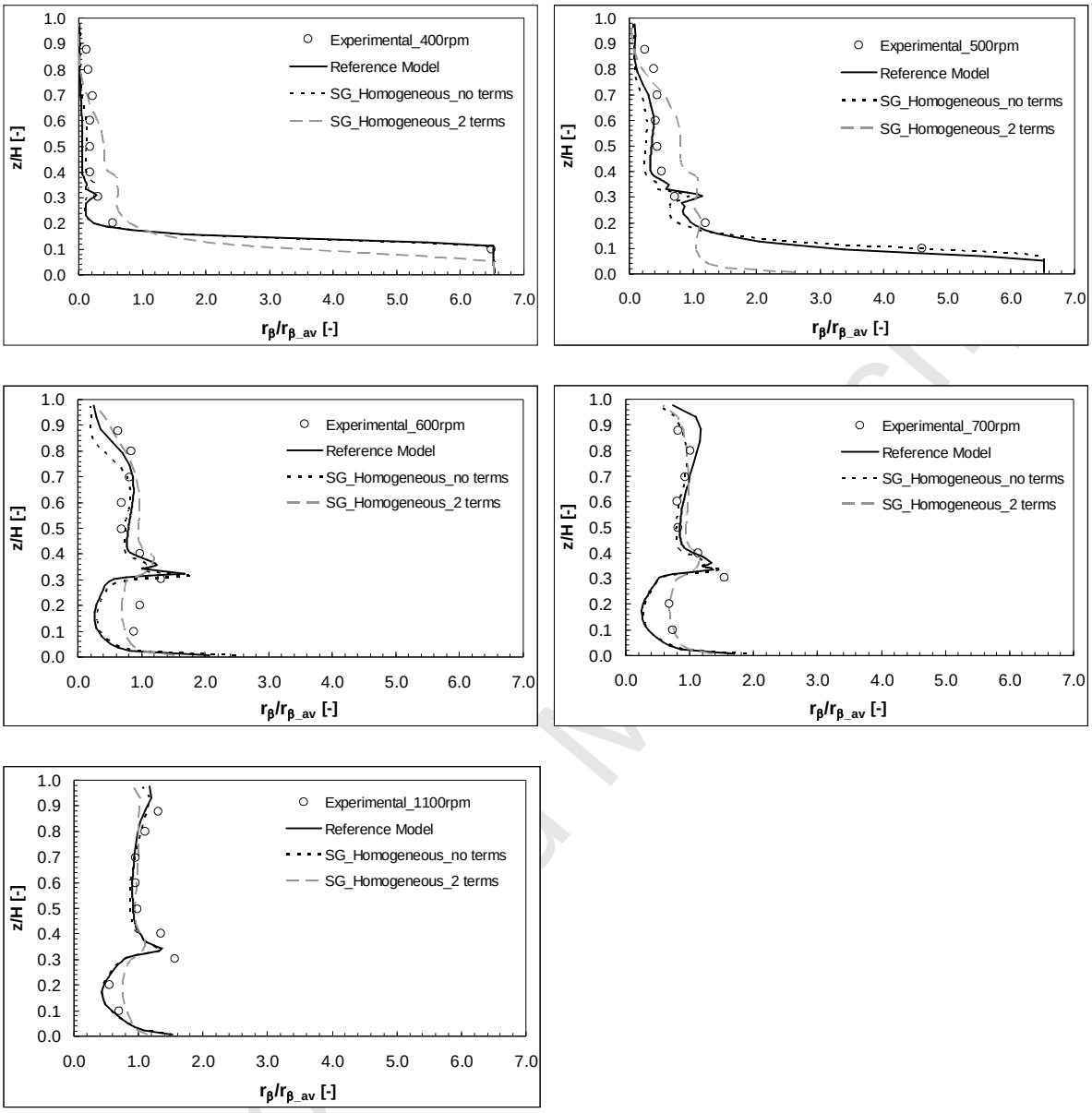

Fig. 19: SG simulations versus steady state local axial profiles of particle concentrations (midway between subsequent baffles and at R = 0.35T) at different impeller speeds for the case of 600-710 μm glass ballottini particles with a solid loading of 25%$^{w/w}$: comparison of different turbulence closures.

6. CONCLUSIONS

Numerical simulations of dense solid-liquid suspensions within flat bottomed vessels stirred by standard Rushton turbines were performed. Different modelling approaches were compared in order to assess their ability to predict the fraction of suspended particles (x_{susp}), the sediment height (h_{sed}) and the particle distribution (r_β *vs* z) at impeller speeds covering the whole range from partial to complete suspension regimes. Different formulations both of the inter-phase drag force and of the turbulence closure were tested. Simulations were carried out with the commercial code Ansys CFX4.4 by adopting the Eulerian-Eulerian Multi Fluid Model.

A very simple CFD model here regarded as the *Reference Model* along with a drag coefficient correction for background turbulence (Brucato et al., 1998) predicted with fair accuracy both the suspension curves and the local axial concentration profiles, although x_{susp} values were somewhat overestimated when large particles were considered.

As regards the modification of the interphase drag force, the *DPE* and the *PwC* approaches were tested, which make use of Gidaspow's correction for dense particle effects and usually can lead to good results when impeller speeds higher than N_{js} are considered (Ochieng and Onyango, 2008; Tamburini et al., 2009a). Conversely, under partial suspension conditions, the use of such correction can lead to an enhancement of the inter-phase drag force causing in turn an over-prediction of x_{susp} and of the particle distribution degree. This effect is especially relevant at intermediate impeller speeds: in fact, when the impeller speed is low, slip velocities are also low so that the dense particle correction does not provide appreciable effects, while at high impeller speeds the solids are more uniformly distributed and, again, drag corrections are of little consequence. Furthermore, for the case of the *PwC* approach, the drag force overestimation within the solid sediment region can further increase because of the adoption of Ergun's equation, despite its use at high local volume fractions is suggested by the literature (CFX-4 Documentation, 1994; Ochieng and Onyango, 2008; Holbeach and Davidson, 2009). In this regard, some cases can be found in the literature where the ad adoption of drag modification due to dense particle effects is found to provide unsatisfactory

predictions (e.g. Wadnerkar et al., 2012). Also, it is very worth noting that all the models tested in the present work include the drag correction due to the background turbulence which in some works is judged as an alternative to the correction for dense particle effects (e.g. Wadnerkar et al., 2012; Ochieng and Onyango, 2008). Clearly, this is conceptually wrong since the two corrections are due to different aspects. However, it is also true that each correction was originally developed in the absence of the other and it remains to be demonstrated whether they can be simultaneously applied in their original form. As an example, the correction of C_D due to the liquid background turbulence is based on the ration d_p/λ: the relation which allows λ to be calculated from ε (eq.10) was formulated for the case of isotropic turbulence, a hypothesis which is questionable in the case of a system with a high solids concentration.

As far as turbulence closure is concerned, adopting the homogeneous k-ε model but neglecting the two additional terms in the continuity equations (*Homogeneous_no terms* approach) yields a good agreement between the predictions and the experimental data as regards the mass fraction of suspended particles and the axial profiles of solid concentration, while it leads to an overestimation of the sediment height (taken midway between two subsequent baffles). Conversely, the adoption of the homogeneous k-ε turbulence model along with the inclusion of the additional turbulence terms in the continuity equations (*Homogeneous_2 terms* approach) leads to large over-predictions of experimental solids volume fractions, thus suggesting that this approach is not suitable to manage incomplete suspensions. The disappointing effect produced by the inclusion of the two terms is rather surprising since these are included to account for the products between the fluctuating volumetric fraction and the fluctuating velocity arising from the Reynolds averaging in the continuity equation. However, it should be observed that the extra-terms in eqs. 25 and 26 are not the exact terms, but rather their diffusive (Boussinesq-like) approximation, which may well be inadequate in the very region where these terms are important, i.e. near the sediment-liquid interface, where anisotropy is large. Therefore, the findings of the present work highlight the need of further studies in order to find an alternative and better way to account for these terms. The

comparison of the present results with ones obtained by an alternative approach based on Favre averaging along with the inclusion of the turbulent dispersion force in the momentum equation may be a good starting point.

On the above grounds, the *Reference Model* (*Asymmetric_no terms*) and *Homogeneous_no terms* approaches were judged as being the most suitable to model partial suspension conditions, with only minor differences between the two. In fact present results show that such two models in which neither dispersion terms in the continuity equation nor drag enhancement corrections for dense-particle effects are included, gives already satisfactory predictions, or even slight overpredictions of the suspended solids fraction (suspension curve). Therefore, it is not surprising that the inclusion of either effect worsens the prediction via an indirect or direct enhancement of the liquid phase's ability to suspend the particles (see discussion in sections 5.2.1a and 5.2.2).

On overall, the results shown in the present work point out a difficulty in the formulation of a single model which is universally capable of reliably and accurately predicting both the amount of unsuspended solids resting on the vessel bottom and the distribution of solid particles within the suspension volume.

Finally, it is worth stressing that the present conclusions are based on a large number of experimental data covering a range of impeller speeds, particle sizes and concentrations, and especially quantities concerning both the solids suspension (i.e. suspension curves and normalized sediment height) and distribution (local axial profiles of solids volume fraction) phenomenon.

ACKNOWLEDGEMENTS

This work was carried out under financial support by Ministero dell'Università e della Ricerca, PRIN-2006 contract n° 2006091953_004: "*Experimental analysis, modelling and simulations of bioslurry reactors for soil remediation*".

NOTATION

Ar	Archimedes number: $Ar = \frac{g d_p^3 \rho_\alpha \left(\rho_\beta - \rho_\alpha\right)}{\mu_\alpha^2}$ (-)
B	impeller blade height (m)
C	impeller clearance (m)
$C_{\alpha\beta}$	inter-phase drag term (kg $m^{-3}s^{-1}$)
C_D	drag coefficient (-)
C_μ, C_1 C_2	k-ε model parameter (-)
D	impeller diameter (m)
d_p	particle mean diameter (m)
g	gravitational constant (m s^{-2})
H	liquid height (m)
h_{sed}	height sediment assumes on the lateral wall midway two subsequent baffles (m)
M	inter-phase momentum transfer term (Nm^{-3})
n	exponent depending on the value of Archimedes number (-)
N	rotational impeller speed (rpm)
N_{js}	just suspension speed (rpm)
N_p	power number (-)
P	pressure (Nm^{-2})
r	volumetric fraction (-)
$r_{\beta\text{-}av}$	average solid volumetric fraction value (-)
r_{β_min}	low cut-off value for the Piecewise correlation approach (-)
r_{β_max}	high cut-off value for the Piecewise correlation approach (-)
$r_{\beta\text{-}packed}$	solid volumetric fraction maximum packing value (-)
R	radial coordinate (m)
Re_p	particle Reynolds number (-)
T	tank diameter (m)
t	time (s)
U	velocity (ms^{-1})
W	baffle width (m)
w/w	mass fraction: w_{solid}/w_{liquid} (%)
x_{susp}	mass fraction of suspended solids (-)
z	axial coordinate (m)

Greek letters

ε	turbulent dissipation (W Kg^{-1})
λ	Kolmogorov length (m)
μ	viscosity (Pa s)
ν	kinematic viscosity (m^2 s^{-1})
ρ	density (Kg m^{-3})
σ	turbulent Prandtl number (-)

Subscripts

α	liquid phase
AS	avoidance of settling
β	solid phase
BL	bottom lifting
t	turbulent

REFERENCES

Angst, R., Kraume, M., 2006. Experimental investigations of stirred solid/liquid systems in three different scales: Particle distribution and power consumption. Chem. Eng. Sci. 61, 2864–2870.

Armenante, P.M., Nagamine, E.U., Susanto, J., 1998. Determination of correlations to predict the minimum agitation speed for complete solid suspension in agitated vessels. Can J Chem Eng 76, 413-419.

Barresi, A., Baldi, G., 1987. Solid dispersion in an agitated vessel. Chem. Eng. Sci. 42, 2949-2956.

Bohnet, M., Niesmak, G., 1980. Distribution of solids in stirred suspensions. Germ. Chem. Eng. 3, 57-65.

Bourne, J.R., Sharma, R.N., 1974. Suspension characteristics of solid particles in propeller-agitated tanks. Proceedings of the First European Conference on Mixing and Centrifugal Separation, Cambridge, BHRA, Cranfield, UK, B3, 25-39.

Brucato, A., Grisafi, F., Montante, G., 1998. Particle drag coefficients in turbulent fluids. Chem. Eng. Sci. 53, 3295-3314.

Brucato, A., Cipollina, A., Micale, G., Scargiali, F., Tamburini, A., 2010. Particle suspension in top-covered unbaffled tanks. Chem. Eng. Sci. 65, 3001–3008.

CFX-4 Documentation. Ansys®, 1994.

Clift, R., Grace, J.R., Weber, M.E., 1978. Bubbles, drops and particles. (Academic Press, New York, San Francisco, London.

Di Piazza, I., Ciofalo, M., 2002. MHD free convection in a liquid-metal filled cubic enclosure. II. Internal heating. International Journal of Heat and Mass Transfer 45, 1493-1511.

Ergun, S., 1952. Fluid Flow through Packed Columns. Chem. Eng. Progress 48, 89-94.

Fan., L., Mao., Z., Wang., Y., 2005. Numerical simulation of turbulent solid-liquid two-phase flow and orientation of slender particles in a stirred tank. Chem. Eng. Sci. 60, 7045-7056.

Feng, X., Li, X., Cheng, J., Yang, C., Mao, Z.-S., 2012b. Numerical simulation of solid-liquid turbulent flow in a stirred tank with a two-phase explicit algebraic stress model. Chem. Eng. Sci., 82, 272-284.

Fletcher, D.F., Brown, G.J., 2009. Numerical simulation of solid suspension via mechanical agitation: effect of the modeling approach, turbulence model and hindered settling drag law. Intern. Jour. of Comp. Fluid Dynam. 23, 173-187.

Gidaspow, D., 1994. Multiphase flow and fluidization, (eds) (Academic Press, San Diego, USA).

Gohel, S., Joshi, S., Azhar, M., Horner, M., Padron, G., 2012. CFD modeling of solid suspension in a stirred tank: Effect of drag models and turbulent dispersion on cloud height. International Journal of Chemical Engineering , art. no. 956975.

Gosman AD, Lekakou C, Politis S, Issa RI, Looney MK., 1992. Multidimensional modeling of turbulent two-phase flows in stirred vessels. AIChE J. ,38 (12),1946-1956.

Hinze, J.H., 1975. Turbulence (McGraw-Hill, New York).

Holbeach, J.W., Davidson, M.R., 2009. An Eulerian-Eulerian model for the dispersion of a suspension of microscopic particles injected into a quiescent liquid. Eng. Appl. Comput. Fl. Mech. 3, 84-97.

Hosseini S., Patel, D., Ein-Mozaffari, F., Mehrvar, M., 2010. Study of solid-liquid mixing in agitated tanks through computational fluid dynamics modelling. Ind. Eng. Chem. Res. 49, 4426-4435.

Jafari, R., Chaouhi, J., Tanguy, P.A., 2012. A comprehensive review of just suspended speed in liquid-solid and gas-liquid-solid stirred tank reactors. Int. J. Chem. Reac. Eng. 10, art. no. R1.

Jirout, T, Moravec, J., Rieger, F., Sinevic, V., Spidla, M., Sobolic, V., Tihon, J., 2005. Electrochemical measurement of impeller speed for off-bottom suspension. Inzynieria chemiczna i procesowa. 26, 485-497.

Jirout,T. and Rieger, F., 2011. Impeller design for mixing of suspensions. Chem. Eng. Res. Des. 89, 1144-1151.

Kasat, G. R.; Khopkar, A. R.; Ranade, V. V.; Pandit, A. B, 2008. CFD simulation of liquid-phase mixing in solid-liquid stirred reactor. Chem. Eng. Sci., 63, 3877-3885.

Kee, R.C.S., Tan, R.B.H., 2002. CFD simulation of solids suspension in mixing vessels. Can. J. Chem. Eng. 80, 721-726.

Khopkar, A.R., Kasat, G.R., Pandit, A.B., Ranade, V.V., 2006. Computational Fluid Dynamics simulation of the solid suspension in a stirred slurry reactor. Ind. Eng. Chem. Res. 45, 4416-4428.

Liu, L., Barigou, M, 2013. Numerical modelling of velocity field and phase distribution in dense monodisperse solid-liquid suspensions under different regimes of agitation: CFD and PEPT experiments. Chem. Eng. Sci., 101, 837-850.

Ljungqvist, M., Rasmuson, A., 2001. Numerical simulation of the two-phase flow in an axially stirred vessel. Chem. Eng. Res. Des., 79, 533-546.

Luo, J.Y., Issa, R.I. and Gosman, A.D., 1994. Prediction of impeller-induced flows in mixing vessels using multiple frames of reference. IChemE Symp. Ser., 136, 549-556.

Mersmann, A., Werner, F., Maurer, S., Bartosch, K., 1998. Theoretical prediction of the minimum stirrer speed in mechanically agitated suspensions. Chem. Eng. Proc., 37, 503–510.

Micale, G., Brucato, A., Grisafi, F., Ciofalo, M., 1999. Prediction of flow fields in a dual-impeller stirred vessel, AIChE Journal 45, 445-464.

Micale G., Carrara V., Grisafi F., Brucato A., 2000. Solids suspension in three phase stirred tanks. Chem. Eng. Res. Des. 78, 319-326.

Micale G., Grisafi F., Brucato A., 2002. Assessment of particle suspension conditions in stirred vessels by means of a Pressure Gauge Technique. Chem. Eng. Res. Des. 80, 893-902.

Micale G., Grisafi F., Rizzuti L., and Brucato A., 2004. CFD Simulation of particle suspension height in stirred vessels. Chem. Eng. Res. Des. 82, 1204-1213.

Micheletti, M., Nikiforaki, L., Lee, K.C., Yianneskis, M., 2003. Particle Concentration and Mixing Characteristics of Moderate-to-Dense Solid-Liquid Suspensions. Ind. Eng. Chem. Res. 42, 6236-6249.

Montante, G., Micale, G., Magelli, F., Brucato, A., 2001. Experiments and CFD predictions of solid particle distribution in a vessel agitated with four pitched blade turbines. Chem. Eng. Res. Des. 79, 1005-1010.

Montante, G. and Magelli, F., 2005. Modelling of solids distribution in stirred tanks: analysis of simulation strategies and comparison with experimental data. Int. Jour Comp. Fluid Dyn. 19, 253-262.

Montante, G., Magelli, F., 2007. Mixed Solids Distribution in stirred vessels: experiments and Computational Fluid Dynamics simulations. Ind. Eng. Chem. Res. 46, 2885-2891.

Montante, G., Paglianti A., Magelli, F., 2012. Analysis of dilute solid-liquid suspensions in turbulent stirred tanks. Chem. Eng. Res. Des. 90, 1448-1456.

Murthy, J.Y., Mathur, S.R., Choudhury, D., 1994. CFD simulation of flows in stirred tank reactors using a sliding mesh technique. IChemE Symp. Ser. 136, 341-348.

Murthy, B.N., Ghadge, R.S., Joshi, J.B,. 2007. CFD simulations of gas-liquid-solid stirred reactor: prediction of critical impeller speed for solid suspension. Chem. Eng. Sci. 62, 7184-7195.

Musil, L., Vlk, J., 1978. Suspending solid particles in an agitated conical-bottom tank. Chem. Eng. Sci., 33, 1123-1131.

Nienow A. W., 1968. Suspension of solid particles in turbine-agitated baffled vessels. Chem. Eng. Sci. 23, 1453-1459.

Ochieng, A., Lewis, A.E., 2006. CFD simulation of solids off-bottom suspension and cloud height. Hydrometallurgy 82, 1-12.

Ochieng, A., Onyango, M. S., 2008. Drag models, solids concentration and velocity distribution in a stirred tank. Powder Tech. 181, 1-8.

Oldshue, J.Y., Sharma, R.N., 1992. The effect of off-bottom distance of an impeller for the 'Just Suspended Speed', Njs. AIChE Symp. Ser. 88, 72-78.

Oldshue, J. Y., 1983, in "Fluid Mixing Technology", Chapter 5, McGraw-Hill, New York**,** NY.

Oshinowo, L.M., Bakker, A., 2002. CFD modeling of solids suspensions in stirred tank. Proceedings of the Conference on Computational Modeling of Materials, Minerals and Metals Processing, 205-215.

Panneerselvam, R., Savithri, S., Surender, G.D., 2008. CFD modeling of gas-liquid-solid mechanically agitated contactor. Chem. Eng. Res. Des. 86, 1331-1344.

Ren, C., Jiang, X., Wang, J., Yang, Y., Zhang X., 2008. Determination of critical speed for complete solid suspension using acoustic emission method based on multiscale analysis in stirred tank. Ind. Eng. Chem. Res. 47, 5323-5327.

Rewatkar V.B., Raghava Rao K.S.M.S., Joshi J.B., 1991. Critical impeller speed for solid suspension in mechanically agitated three-phase reactors. 1.Experimental part. Ind. Eng. Chem. Res. 30, 1770-1784.

Rieger, F., 2000. Effect of particle content on agitator speed for off-bottom suspension. Chem. Eng. J. 79, 171-175.

Rieger, F., Ditl, P., Havelkova, O., 1988. Suspension of solid particles – Concentration profiles and particle layer on the vessel bottom. Proceedings of the 6th European Conference on Mixing, Pavia, Italy, 24-26 May, 251-258.

Sardeshpande, M.V., Sagi, A.R., Juvekar, V.A., Ranade, V.V., 2009. Solid suspension and liquid phase mixing in solid-liquid stirred tanks, Ind. Eng. Chem. Res. 48, 9713-9722.

Sardeshpande, M.V., Juvekar, V.A., Ranade, V.V., 2011. Solid suspension in stirred tanks: UVP measurements and CFD simulations, Can. Jour. Chem. Eng. 89, 1112-1121.

Scully, J., Frawley, P., 2011. Computational Fluid Dynamics analysis of the suspension of nonspherical particles in a stirred tank. Ind. Eng. Chem. Res. 50, 2331-2342.

Selima, Y.S., Fangary, Y.S., Mahmoud, N.A., 2008. Determination of minimum speed required for solids suspension in stirred vessels using pressure measurements. Can. Jour. Chem. Eng. 86, 661-666.

Tamburini, A., 2011. Suspension phenomena in solid-liquid agitated systems. Doctoral Thesis, University of Palermo. Fotograf, Palermo, Italy. ISBN: 9788895272979.

Tamburini, A., Cipollina, A., Micale, G., Ciofalo, M., Brucato, A., 2009a. Dense solid–liquid off-bottom suspension dynamics: simulation and experiment, Chem. Eng. Res. Des. 87, 587–597.

Tamburini, A., Gentile, L., Cipollina, A., Micale, Brucato, A., 2009b. Experimental investigation of dilute solid-liquid suspension in an unbaffled stirred vessels by a novel pulsed laser based image analysis technique. Chem. Eng. Transactions 17, 531-536.

Tamburini, A., Cipollina, A., Micale, G., Brucato, A., Ciofalo, M., 2011a. CFD Simulations of dense solid-liquid suspensions in baffled stirred tanks: predictions of suspension curves. Chem. Eng. J. 178, 324-341.

Tamburini, A., Cipollina, A., Micale, G., 2011b. CFD simulation of solid liquid suspensions in baffled stirred vessels below complete suspension speed**.** Chemical Engineering Transactions 24, 1435-1440.

Tamburini, A. Cipollina, A., Micale, G., Brucato, A., 2011c. Dense solid-liquid suspensions in top-covered unbaffled stirred vessels. Chemical Engineering Transactions 24,1441-1446.

Tamburini, A., Cipollina, A., Micale, G., Brucato, A., Ciofalo, M., 2012a. CFD simulations of dense solid-liquid suspensions in baffled stirred tanks: prediction of the minimum impeller speed for complete suspension. Chem. Eng. J. 193-194, 234-255.

Tamburini, A., Brucato, A., Cipollina, A., Micale, G., Ciofalo, M., 2012b. CFD predictions of sufficient suspension conditions in solid-liquid agitated tanks. International Journal of Nonlinear Sciences and Numerical Simulation 13, 427–443.

Tamburini, A., Cipollina, A., Micale, G., Brucato, A., 2012c. Measurements of Njs and power requirements in unbaffled bioslurry reactors. Chemical Engineering Transactions 27, 343-348.

Tamburini, A., La Barbera, G., Cipollina, A., Ciofalo, M., Micale, G., 2012d. CFD simulation of channels for direct and reverse electro dialysis. Desalination and Water Treatment 48, 370-389.

Tamburini, A., Cipollina, A., Micale, G., Brucato, A., 2013a. Particle distribution in dilute solid-liquid unbaffled tanks via a novel laser sheet and image analysis technique. Chem. Eng. Sci. 87, 341-358.

Tamburini, A., Brucato, A., Cipollina, A., Micale, G., Ciofalo, M., 2013b. CFD simulations of dense solid-liquid suspensions in baffled stirred tanks: prediction solid particle distribution. Chem. Eng. J. 223, 875–890.

Tamburini, A., Cipollina, A., Micale, G., Brucato, A., Ciofalo, M., 2013c. CFD prediction of solid particle distribution in baffled stirred vessels under partial to complete suspension conditions. Chemical Engineering Transactions 32, 1447-1452.

Tatterson, G. B., 1991. Fluid Mixing and Gas Dispersion in Agitated Tanks. McGraw-Hill: New York.

Van der Westhuizen, A.P. and Deglon, D.A., 2007. Evaluation of solids suspension in a pilot-scale mechanical flotation cell: The critical impeller speed. Minerals Engineering 20, 233-240.

Wadnerkar, D., Utikar, R.P., Tade, M.O., Pareek, V.K., 2012. CFD simulation of solid-liquid stirred tanks. Advanced Powder Technology, 23, 445-453.

Wang, F., Mao, Z., Shen, X., 2004. Numerical study of solid-liquid two-phase flow in stirred tanks with Rushton impeller. (II) Prediction of critical impeller speed. Chinese J. Chem. Eng. 12, 610-614.

Wang, L., Zhang, Y., Li, X., Zhang, Y., 2010. Experimental investigation and CFD simulation of liquid-solid-solid dispersion in a stirred reactor. Chem. Eng. Sci. 65, 5559-5572.

Wang, S., Boger, D.V., Wu, J., 2012. Energy efficient solids suspension in an agitated vessel-water slurry. Chem. Eng. Sci. 74, 233-243.

Yamazaki, H., Tojo, K., Miyanami, K., 1986. Concentration profiles of solids suspended in a stirred tank. Powder Tech. 48, 205-216.

Zhao, H., Zhang, T., Liu, Y., Zhang, Z., Zhao, C., 2013. Numerical simulations of solid-liquid stirred tank with an improved Intermig impeller. AIP Conference Proceedings, 1542, 1286-1289.

Zhu, Y. and Wu, J., 2002. Critical impeller speed for suspending solids in aerated agitation tanks. Can. Jour. Chem. Eng. 80, 682-687.

Zwietering T. N., 1958. Suspending of solid particles in liquids by agitators, Chem. Eng. Sci. 8, 244-253.